✧ *Author Response to Referee comments*

#Referee comment 1

General comments:

The manuscript entitled “Preflight Calibration of the Chinese Environmental Trace Gases Monitoring Instrument (EMI)” by Zhao et al. describes the method of the preflight wavelength and radiometric calibration efforts for the EMI instrument. Moreover, it provides an estimate of the expected, on-orbit signal to noise ratio for one particular solar zenith angle. In my opinion, this manuscript provides valuable information to the community, but requires careful modifications before it is published. My detailed comments are:

(1) There are several editorial and vocabulary issues, possibly due to a language barrier, that make the manuscript hard to read and sometimes result in the incorrect meaning. Please proof-read the manuscript carefully. Several examples are listed in the following:

a. “integral time” should be “integration time”

b. The symbol “～” is used throughout the manuscript to describe “from/to” intervals or ranges. The correct symbol to use is “-“.

c. The word “data” is used to describe “measurements”. For example, “: : :determined by 20 spectral response data: : :” should be modified to “determined using 20 spectral response measurements: : :”. Similarly, “One hundred observed data is obtained: : :” should be modified to read: “One hundred measurements were obtained: : :”

d. “: : :the spectral response function is better than 0.03nm.” should be modified to “the full width at half maximum (FWHM) of the instrumental line shape function is less than 0.03nm.”

e. Throughout the manuscript, the abbreviation “FWHM” is used for the FWHM of the instrumental line shape function (ILS). Whenever it is used, it has to be made clear that it describes the ILS and not the width of some other function.

f. In section 3, gain steps between 0-63 are introduced which result in different gain values within the CCD readout electronics (A/D converter). However, the word “Gain” is used for the digital gain steps and the word “magnification” is used for the actual gain value. I strongly encourage the authors to describe the values 0-63 as “gain steps” (or something similar) and the factor with which the raw signal is multiplied as “gain” or “gain value”. In the community, the word “magnification” is almost exclusively used for optical magnifications, which can result in confusion here. Please do not use “magnification” in this context.

g. The words “accuracy” and “precision” (and sometimes “non-stability” or “variety”) are sometimes used interchangeably and often wrongly in this manuscript. Please familiarize yourself with the different meanings of accuracy and precision and use them appropriately. Do not use non-stability or variety.

h. I assume the CCD names are “e2v: : :” not “EV2: : :”

i. The dark signal is incorrectly defined in line 288. The common way to define the signal that is obtained when no photons enter the instrument is to add the “bias value” and the “dark signal”, where the dark signal is the dark current multiplied by the integration time. The dark noise is typically the noise component that is caused by this dark signal, in this case, the shot noise of the dark signal.

j. Figure number is missing in line 366.

k. The unit Watt is typically abbreviated with a capital “W”, not a lower case “w”.

l. Equation number is missing in line 428. In fact, the equations are not numbered at all. Please assign equation numbers to all equations.

m. Please use the greek letter μ to indicate thousandths not the letter u.

n. Figure number is missing in line 430.

Response:

Many thanks for the careful and professional commenting. Firstly, the comments a-n have been corrected in the paper. Secondly, the paper is carefully modified.

Author's changes in revised manuscript: the entire manuscript is carefully modified

(2) It is not sufficiently clear what the wavelength shifts shown in Figure 3 are. Do they represent an additional offset that is included in the polynomial function which is determined for the center?

Response:

The wavelength shifts in Figure 3 are measured by the tunable laser in the spatial dimension with the interval of 5°.

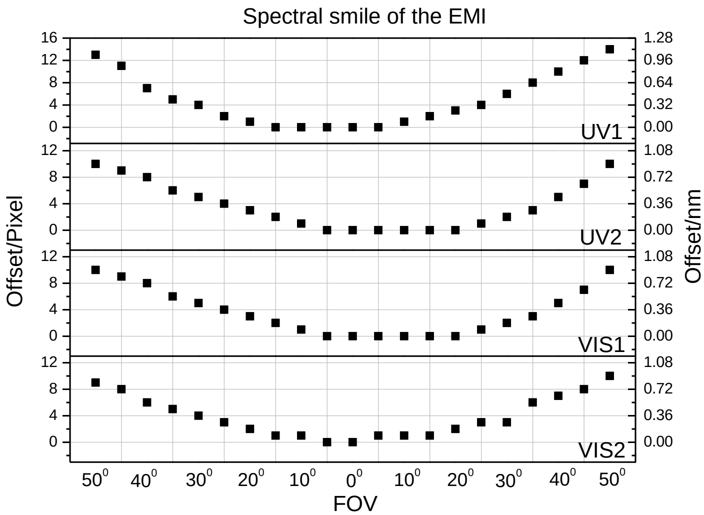

The wavelength (pixel) shift enlarges from the CFOV to the edge FOV. The UV1, UV2, VIS1, and VIS2 wavelength (pixel) shifts of the edge FOV are 1.12 nm (14 pixels), 0.9 nm (10 pixels), 1.2 nm (10 pixels), and 1.3 nm (10 pixels), correspondingly. For the L1b processor of the EMI， the spectral smile effect will be calibrated using a spectrum-matching technique.

Author's changes in revised manuscript: Line 143-149

(3) The manuscript states that the CCDs for the visible channels do not have any temperature control. Since the dark current depends strongly on the CCD temperature, it would be very helpful to quote the expected temperature variations of these detectors throughout the orbit and as a function of orbit beta angle. In addition, it would be helpful to refer to the strategy of periodic dark measurements at this point, so the reader understands how this potential problem is mitigated.

Response:

The CCDs for the visible channels do not have independent temperature control, but they work in a constant temperature environment. The temperature is similar to that in the visible spectrometer, which has temperature control. Thus, the change of CCD temperature is not a problem.

Author's changes in revised manuscript: Line 308-310

(4) The authors state: “The offset is fairly const, *: : :*” I believe they mean “The bias value is constant,*: : :*” This is generally a good assumption for well-designed electronics. Have the authors quantified the precision of the bias values?

Response:

The read-out register within the CCD has an excess of 16 blank pixels, which can be used to measure the electronic offset on the ground. The measurements show that the offset is not constant but drifts with time (about 0.5%). Therefore, the electronic offset is obtained per measurement frame in-orbit, and the electronic offset correction is implemented in the L1b data processor.

Author's changes in revised manuscript: Line 316-319

(5) I do not understand the traces in the top two panels of Figure 8. For a constant dark current and a constant bias value, the difference between the measurements with 0.5s and 1.0s integration time should be half of the difference between the measurements with 1.0s and 2.0s integration time. Please explain.

Response:

The pixels in the readout register cannot be used to accomplish the binning due to the full well limitation. In this case, the pixel binning is accomplished in the Field Programming Gate Array. Fast readout frequency is needed for the process. The fast readout frequency leads to signal distortion. Therefore, the difference between the measurements with 0.5 and 1.0 s integration times is not half of the difference between the measurements with 1.0 and 2.0 s integration times. Based on the signal distortion, we have obtained absolute radiance calibration key data at different integration time on the ground. The calibration key data are used for the L1b data processor.

Author's changes in revised manuscript: Line 328-335

(6) A reference for MODTRAN should be included

Response:

A reference for MODTRAN have been included in the paper.

Author's changes in revised manuscript: Line 436

(7) The denominator of the equation on line 414 should be the standard deviation.
Thus, the term in the sum needs to be squared. I assume that the actual calculations
were performed correctly.

Response:

The equation in the paper has been corrected. We have confirmed that the actual calculations were performed correctly.

Author's changes in revised manuscript: Line 461

(8) The authors state that the measured SNR in figure 13 is departing from the simulation between 460-500nm due to lower transmittance of the instrument (filter) in this range. However, if the equation in line 394 includes the proper transmission function, this effect should be included in the simulation. Please explain.

Response:

The equation in line 394 includes the proper transmission function. But for the SNR-simulation, the transmittance of the filter is not included as we want to analyze the effect of the filter on SNR. The simulation SNR included the effect of the filter is shown in following figure.

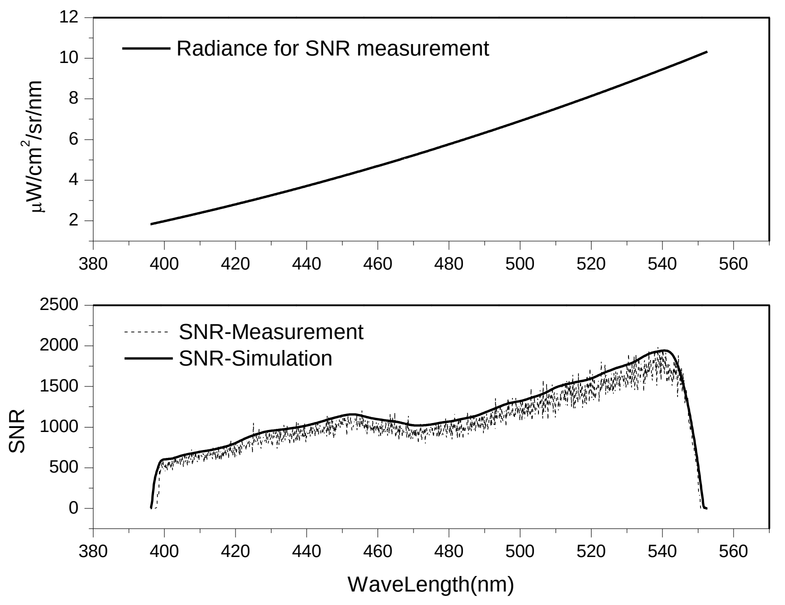

Author's changes in revised manuscript: Line 463-464

(9) It is not clear to me how the PRNU can provide a significant contribution to the lower than expected SNR, unless it is varying in time (line 432). Please explain.

Response:

The PRNU is not varying during the SNR measurement, and will not provide a significant contribution to the lower than expected SNR. There are two main factors: the light source for the SNR measurement and the pixel response of the EMI. The PRNU has been corrected in the paper.

Author's changes in revised manuscript: Line 476

(10) If I understand correctly, the pre-flight, radiometric calibration of EMI was not conducted under flight-like vacuum and possibly thermal conditions. If this is the case, please address in more detail how the in-flight calibration will be used to accomplish absolute radiometric calibration of the flight data.

Response:

The pre-flight, radiometric calibration of EMI was not conducted under flight-like vacuum and possibly under thermal conditions due to the limitation of the calibration facility. The EMI on-ground response to the quartz tungsten halogen WLS (6 V, 10 W) is displayed in following figure, which uses UV2 and VIS1 as examples.

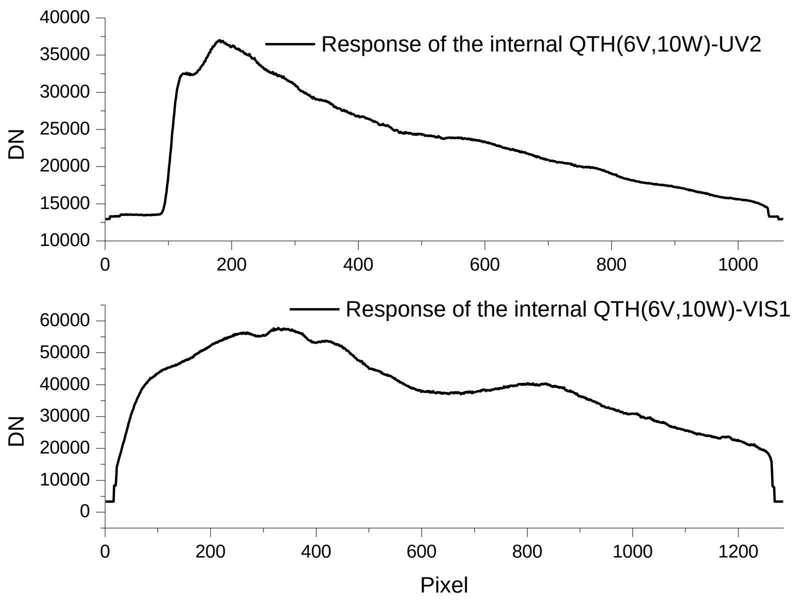

The EMI in-orbit response to the quartz tungsten halogen will be obtained after the launch. The change between the on-ground and in-orbit responses is used to correct the preflight radiometric calibration, which in turn is used to accomplish the in-flight absolute radiometric calibration of the flight data.

Author's changes in revised manuscript: Line 386-394

(11) Finally, while the manuscript shows the performance of the instrument on the ground, the reader is not told what the actual performance requirements are. Presumably, the instrument performance requirements are driven by the scientific objectives. Comparing the measured/estimated performance (e.g. SNR) with the mission requirements would make the conclusion much stronger.

Response:

We have added the performance requirements to the introduce section and added the on-ground calibration results in the conclusions section.

Performance requirements

Spectral range: UV1:240–315 nm; UV2:311–403 nm; VIS1:401–550 nm; VIS2: 545–710 nm;

Spectral resolution: <0.55 nm;

Accuracy of the on-ground wavelength calibration: <0.05 nm;

Accuracy of the on-ground radiometric calibration: <5%;

SNR:

UV channel: >200 (@1.27 $\mu W / cm^2 / sr / nm$)

VIS channel: >1300 (@10.89 $\mu W / cm^2 / sr / nm$)

Conclusions

The spectral and radiometric response performance of the EMI is obtained by preflight calibration. The on-ground calibration results are shown as follows:

Spectral calibration results:

UV1: 236.44–317.28 nm with the spectral resolution ≤0.45 nm;

UV2: 306.08–407.12 nm with the spectral resolution ≤0.49 nm;

VIS1: 395.50–552.63 nm with the spectral resolution ≤0.48 nm;

VIS2: 534.63–712.90 nm with the spectral resolution ≤0.49 nm;

The final accuracy of the wavelength calibration is <0.05 nm.

Radiometric calibration results:

UV1: 4.64%, UV2: 4.63%, VIS1: 4.43%, VIS2: 4.42%.

The on-ground calibration results meet the performance requirements of the EMI.

The EMI in-orbit simulation $SNR_{simulation}$ is obtained by the radiance $R_{simulation}$ at an albedo of 0.3 and solar zenith of 60°. The in-orbit simulation SNR at the radiance of 1.27/10.89 $\mu W/cm^2/sr/nm$ can be achieved by the following equation:

$$SNR = SNR_{simulation} \cdot \sqrt{\frac{R}{R_{simulation}}},$$

where R is 1.27 for UV channels and 10.89 $\mu W/cm^2/sr/nm$ for VIS channels.

For the in-orbit simulation SNR at the radiance of 1.27/10.89 $\mu W/cm^2/sr/nm$, the results are presented in the following table.

In-orbit simulation SNR at the requirement radiance

Channel		**SNR (simulation)**	**SNR (requirements)**
UV2	330nm	328	200
	360nm	356	200
	390nm	388	200
VIS1	420nm	1860	1300
	480nm	1900	1300
	540nm	2040	1300
VIS2	560nm	2200	1300
	620nm	2300	1300
	680nm	2400	1300

Author's changes in revised manuscript: Line 486-506

#Referee comment 2

General comments:

The paper by Zhao et al. reports on the preflight calibration of the Chines Environmental Trace Gases Monitoring Instrument (EMI). Wavelength calibration of the instrument, a thermal vacuum test to investigate the impact of in-orbit conditions on the whole system and the radiometric calibration are described in detail and results are shown. Furthermore, the expected signal-to-noise ratio for each channel has been estimated using model calculations.

This review refers to the modified manuscript submitted by the authors on June 30. The manuscript is in general clearly written and I recommend it for publication in AMT. However, the authors should consider following comments and recommendations.

(1) Section on performance requirements: The authors should give some information on what these requirements based on. I recommend putting the information either in a table or in proper sentences. Please add this section after the general instrument description.

Response:

Large spectral range from 240 nm to 710 nm combined with high spectral resolution(0.3 nm to 0.5 nm) of the EMI enables the measurement of several trace gases(e.g., NO2, O3, SO2, BrO, HCHO) as well as aerosol, see table 2. To achieve a high retrieval precision, a high SNR is required for the scattered radiance from the UV to the VIS.

Table 2. EMI data products.

Product Name	**Wavelength Band/nm**
O3	300-345(UV1,UV2)
SO2	305-330(UV1,UV2)
NO2	425-500(VIS1)
BrO	344-360(UV2)
HCHO	335-360(UV2)
Aerosol	UV2,VIS1,VIS2

Author's changes in revised manuscript: Line 97-101

(2) Instrument description: I'm wondering, why the expected spatial resolution in the Visible is smaller than in the UV since the expected intensity should be larger.

Response:

CCD for the Visible has 576 pixels in the spatial range, each pixel measuring $22.5 \times 22.5\, um^2$.

CCD for the UV has 1032 pixels in the spatial range, each pixel measuring $13 \times 13\, um^2$. Calibration results show that:

- Spatial resolution in the Visible is 12km on electronic binning of 4, and is 48km on electronic binning of 16.
- Spatial resolution in the UV is 8km on electronic binning of 4, and is 48km on electronic binning of 24.

No changes in revised manuscript

(3) Thermal vacuum test: I'm wondering about the relatively small temperature range investigated in this study. Is this really something to expect in reality?

Response:
The in-orbit results showed that temperature stability is better than 0.1K. Actually, the temperature investigated in this study has been applied to EMI after launch.

No changes in revised manuscript

(4) Radiance calibration, Dark signal: The authors stated, that the spectrometer in the Visible has temperature control and changes of the CCD are therefore not an issue. Again, the question: Is this true under real in-orbit conditions e.g. when the system comes from the dark to the illuminated part of the orbit?

Response:
An investigation done after launch shows that the temperature stability is better than 0.1K over one orbit. This temperature variation over the orbit leads to very small change of the background signal.

Author's changes in revised manuscript: Line 310-312

(5) SNR (do not use an acronym in the caption): Table 8 and also some sentences concerning the SNR should move from the Conclusions section to the SNR section. In general, I'm a bit unsettled that the assumption of an albedo of 0.3 in the SNR simulations is useful. For most of the relevant scenes the albedo is much lower!

Response:
a) Table 8 and the sentences concerning the SNR have been moved from the Conclusions section to the SNR section.
b) The SNR at albedo of 0.3 is typical SNR of the EMI. SNR at other albedo can be obtained from the typical SNR by equation(16) in the paper:

$$SNR = SNR_{simulation} \cdot \sqrt{\frac{R}{R_{simulation}}}$$

Author's changes in revised manuscript: Line 486-494

Minor corrections

• Line 11, please change to launch date

Changed (date:2018.05.09)

Author's changes in revised manuscript: Line 11,37

• Line 25f: Check sentence for clarity

Modified.

Author's changes in revised manuscript: Line 25

• Line 29f: Check citations - I recommend to use following publications instead:

Burrows et al.: The global ozone monitoring experiment (GOME): Mission concept and first scientific results, 1999

Bovensmann et al.: SCIAMACHY: Mission objectives and measurement modes, 1999

Levelt et al., The Ozone Monitoring Instrument, 2006

Changed

Author's changes in revised manuscript: Line 28,29

• Line 96: travels instead of travel

Corrected

Author's changes in revised manuscript: Line 95

• Line 145: …considered as a Gaussian-type function …

Corrected

Author's changes in revised manuscript: Line 150

• Line 155: … and the accuracy of the FWHM ..

Corrected

Author's changes in revised manuscript: Line 160

• Line 161f: A mercury argon lamp is used as light source for EMI …

Corrected

Author's changes in revised manuscript: Line 166,167

• Figures 5 and 6: What is NTC??

Corrected (NTC: No Temperature control)

Author's changes in revised manuscript: Line 185

• Line 207: … are presented ...

Corrected

Author's changes in revised manuscript: Line 215

• Line 224: Write solar calibration mode (SCM) in caption

Corrected

Author's changes in revised manuscript: Line 232

• Line 279: Table missing?

Added

Author's changes in revised manuscript: Line 287

• Line 308: about 0,5% per what??

Updated.

Author's changes in revised manuscript: Line 318

• Line 316, Figure 8: … for … instead of … under …

Corrected

Author's changes in revised manuscript: Line 326

• Line 332: … check sentence for clarity …

Modified.

Author's changes in revised manuscript: Line 342

• Line 346f: Check numbers given here!!

Corrected

Author's changes in revised manuscript: Line 354

• Line 358: Based …

Corrected

Author's changes in revised manuscript: Line 365

• Line 429f: … have been discussed elsewhere …

Corrected

Author's changes in revised manuscript: Line 437

• Line 450: … are recorded …

Corrected

Author's changes in revised manuscript: Line 457

• Line 467f: .. of the SNR … and check sentence for clarity

Modified.

Author's changes in revised manuscript: Line 469-470

• Line 470f: I’m not sure, what the authors would like to point out here.

Modified

Author's changes in revised manuscript: Line 469-470

• Line 472: The simulation of the … in the UV2, … channels are …

Corrected

Author's changes in revised manuscript: Line 478

• Line 473: … of channel UV1 …

Corrected

Author's changes in revised manuscript: Line 479

• L481f: Numbers given here are different to numbers in Table 8!

Response: The numbers in L481f are obtained by the radiance at an albedo of 0.3 and solar zenith of 60 °. The numbers in table 8 are obtained by the radiance of 1.27/10.89 $\mu W / cm^2 / sr / nm$

No changes in revised manuscript

✧ *Marked-up manuscript version*

Preflight Calibration of the Chinese Environmental Trace Gases Monitoring Instrument (EMI)

MinJie Zhao, FuQi Si, HaiJin Zhou, ShiMei Wang, Yu Jiang, WenQing Liu

Key ~~laboratory~~Laboratory of Environmental Optics and Technology, Anhui Institute of Optics and Fine Mechanics, Chinese Academy of Sciences, Hefei~~,~~ 230031, China

Correspondence to: FuQi Si (sifuqi@aiofm.ac.cn)

Abstract

~~The~~An Environmental trace gases Monitoring Instrument (EMI) is a nadir-viewing wide-field imaging spectrometer, ~~aiming~~which aims to quantify the global distribution of tropospheric and stratospheric trace gases, ~~which~~and is planned to be launched in 2018.05.09. The selected wavelength bands for EMI are ultraviolet channels: UV1 (240~~-315nm~~ –315 nm), UV2 (311~~-403nm),~~ –403 nm) and visible channels: VIS1 (401~~-550nm)~~ –550 nm), and VIS2 (545~~-710nm), the~~ –710 nm). The spectral resolution is 0.3~~-~~–0.~~5nm~~5 nm, and the swath is ~~about~~approximately 114~~ degrees~~ ° wide to achieve a one-day global coverage. The preflight calibration of the EMI is discussed in this paper. Tunable laser and rotating platform are adopted for ~~the~~an EMI wavelength calibration of the ~~whole~~entire field of view. The accuracy of the wavelength calibration is ~~better~~less than 0.~~05nm~~05 nm. In addition, the ~~calibration data in the Sun~~solar calibration mode shows ~~that~~ the same ~~calibration~~ results ~~are obtained~~ compared with ~~the~~ Earth observation mode. ~~In order~~A thermal vacuum test is performed to investigate the influence of in-orbit thermal~~-~~ vacuum conditions on the EMI, ~~the thermal vacuum test is performed, and the~~and EMI spectral response changes with pressure, optical bench temperature, and charge-coupled device (CCD) detector temperature are obtained. For ~~the~~a radiometric calibration of UV1, ~~the diffuse~~a diffuser plate

with a ~~1000W~~1000 W xenon lamp~~ is chosen~~, which produces a sufficient ~~ultraviolet~~UV output~~. And the,~~ is selected. An integrating sphere system with tungsten halogen lamp is selected for the UV2, VIS1, and VIS2. The ~~accuracy~~accuracies of ~~the~~ radiance calibration ~~is~~are 4.53~~%(~~% (UV1), 4.52~~%(~~% (UV2), 4.31~~%(~~% (VIS1~~)~~), and 4.30~~%(~~% (VIS2). The goniometry correction factor and irradiance response coefficient of the EMI are also calibrated on the ground for ~~the~~an in-orbit calibration of the solar.~~ As the effect of Signal~~ A signal-to~~-Noise~~-noise ratio (SNR)~~ on the retrieved results, a SNR~~ model of the EMI is introduced, and the EMI in-orbit SNR is estimated using the SNR ~~model~~ and~~ the~~ MODTRAN radiance ~~model~~models.

1 Introduction

~~A series of~~Numerous space-borne spectrometers~~ like~~, such as GOME~~[~~*~~A.Hahne~~* [*JOHN P. BURROWS et al.,* *~~1993~~1999*], SCIAMACHY~~[~~*~~S. Noel~~* [*H. BOVENSMANN et al.,* *~~1998~~1999*], GOME-2 [*Rosemary Munro~~,~~ et al., 2016*~~]~~], and OMI~~[~~*~~Pawan K Bhartia~~* [*Pieternel F. Levelt et al., 2006*~~]~~], have been successfully applied to the global monitoring of atmospheric trace gas distributions. These instruments measure sun radiance backscattered from the Earth's atmosphere in the UV-VIS wavelength range. ~~The~~ TROPOMI builds upon the heritages of ~~the~~ **S**CIAMACHY and ~~the~~ OMI instruments, which ~~was~~were launched in 2017 on ~~ESA's~~ESA's Sentinel 5 precursor satellite [*Rovert Voors et al., 2012*].

~~The~~An Environmental trace gases Monitoring Instrument (EMI) is a space-borne nadir-viewing wide-field imaging spectrometer, which is used to obtain global distributions of tropospheric and stratospheric trace gases (e.g~~.~~., NO2, O3, HCHO, and SO2) at high spatial and spectral resolution. The EMI is planned to be launched in 2018.05.09.

Performance requirements

Spectral range: UV1:240–315 nm; UV2:311–403 nm; VIS1:401–550 nm; VIS2: 545–710 nm;

Spectral resolution: <0.5 nm;

Accuracy of the on-ground wavelength calibration: <0.05 nm;

Accuracy of the on-ground radiometric calibration: <5%;

SNR:

UV channel: >200 (@1.27 $\mu W / cm^2 / sr / nm$)

VIS channel: >1300 (@10.89 $\mu W / cm^2 / sr / nm$)

Instrument description

The EMI has four spectral channels~~(~~ (i.e., UV1, UV2, VIS1, and VIS2) ~~ranging~~that range from

240 nm to 710 nm. Each channel adopts an Offner imaging spectrometer~~,~~ and ~~two-dimensional~~2D charge-coupled device detectors. The EMI enables an instantaneous field of view (FOV) of 114° (corresponding to a 2600 km broad swath on the ~~Earth's~~Earth’s surface), and the space resolution is either ~~8km/12km~~8 km/12 km (UV/VIS channel) or ~~48km~~48 km (UV~~,~~ and VIS ~~channel~~channels) at nadir, depending on ~~the~~an electronic binning factor~~, see table 1. And~~ (Table 1). Moreover, a one-day global coverage can be realized. The anticipated lifetime of the EMI is ~~eight~~8 years, and its properties are ~~shown~~listed in Table 1.

Table 1. EMI instrument properties

~~**Spectral range**~~	~~UV1: 240-315nm; UV2: 311-403nm~~
	~~VIS1: 401-550nm; VIS2: 545-710nm~~
Spectral sampling	UV1: 0.~~08nm;~~ 08 nm; UV2: 0.~~09nm~~09 nm
	VIS1: 0.~~12nm;~~ 12 nm; VIS2: 0.~~13nm~~13 nm
Spectral resolution~~(FWHM)~~	0.3~~-~~ – 0.~~5nm~~5 nm
Telescope swath IFOV	114~~ degrees~~ ° (2600 km on the ground)
Telescope flight IFOV	0.5~~ degrees~~ ° (6.5 km on the ground)
CCD detectors	UV: 1072 × 1032 (spectral × spatial) pixels
	VIS: 1286 × 576 (spectral × spatial) pixels
Ground pixel size at the nadir	~~13km × 48km~~13 km × 48 km (electronic binning factor
	UV: 24, VIS: 16)
	~~13km × 8km~~13 km × 8 km (UV, binning factor 4)
	~~13km × 12km~~13 km × 12 km (VIS, binning factor 4)
Orbit	Polar, sun-synchronous; Orbit period: 98 ~~minutes~~min, 53 ~~seconds,~~s; Ascending node equator crossing time: 13:30~~ PM~~

The optical layout of the EMI is ~~shown~~illustrated in Fig. 1. The EMI consists of a telescope and four spectrometers.

The telescope provides an instantaneous ~~field of view~~FOV of 114° in the swath direction and ~~of~~ 0.5°

in the flight direction, which yieldthereby yielding an overall ground coverage of about 2600km byapproximately 2600 km × 6.5km5 km at an altitude of 705km705 km. The spatial resolution in the swath direction dependsand flight directions depend on the electronic binning factor, in the flight direction depending on the and CCD integralintegration time, respectively. Four Offner imaging spectrometers are adopted by the EMI, where each spectrometer withhas a convex grating and a 2-dimensional2D CCD detectors. The Offner imaging spectrometer is easy tocan be easily miniaturized and is lightweight, and is suitable for the development of space technology. ItThis spectrometer is also suitable for high spatial and spectral resolution detection systems. The EMI covercovers a 240-710nm–710 nm range with thea spectral resolution of 0.3-–0.5nm5 nm.

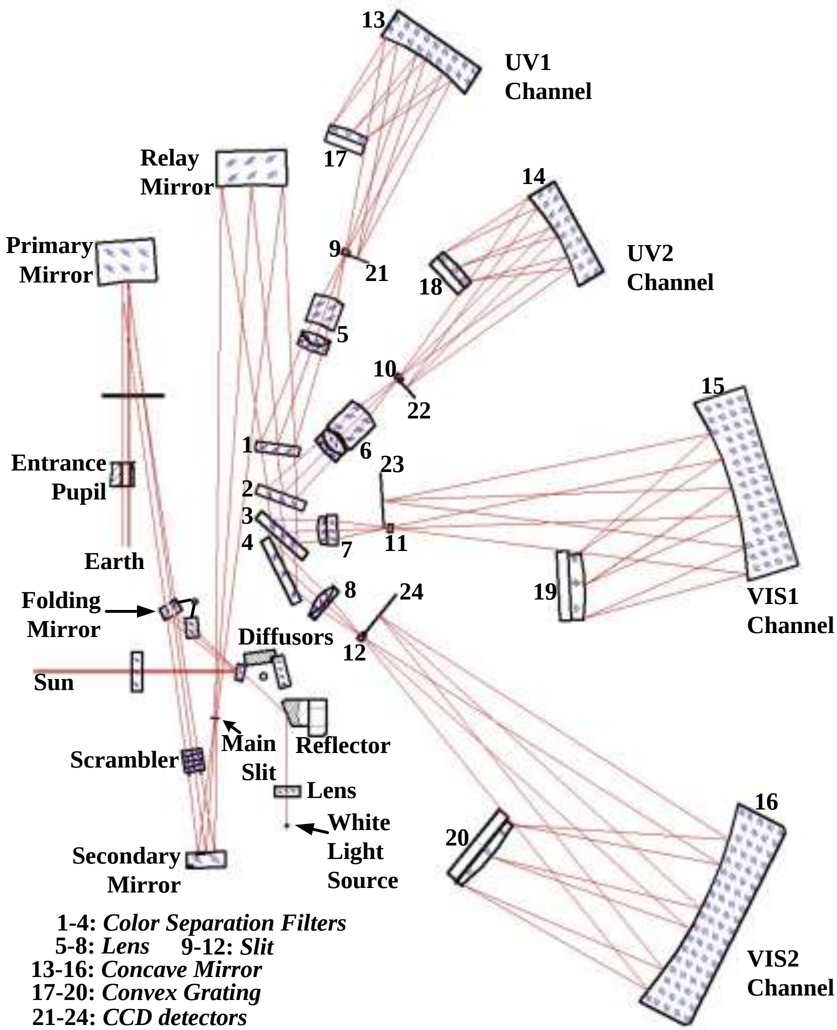

Fig.1. Optical layout of the EMI instrument

One observation mode and two calibration modes are ~~include~~included in the EMI. The observation mode is used to detect ~~the~~ atmospheric scattering light, and the two calibration modes are utilized for in-orbit calibration.

In the observation mode, the Earth radiance enters the telescope ~~via~~through the entrance pupil~~,~~ and is imaged on the main slit after reflection by the primary and secondary ~~mirror~~mirrors. A polarization scrambler is located before the secondary mirror, which is used to ~~make~~enable the EMI to be insensitive to the polarization state of the incident light. ~~Behind~~Furthermore, a relay mirror behind the main slit ~~a relay mirror~~ reflects the incident light on ~~the color~~Color separation ~~filter~~filters 1~~-~~–4. ~~The color~~Color separation filter 1 reflects the 240~~-315nm~~–315 nm range of the spectrum to the UV1 channel and transmits the rest of ~~spectrum~~the spectra to ~~the color~~Color separation filter 2. ~~As a result~~Consequently, 311~~-403nm~~–403, 401~~-550nm~~–550, and 545~~-710nm range~~–710 nm ranges of the ~~spectrum~~spectra are reflected to the UV2, VIS1, and VIS2 ~~channel~~channels by ~~the filter~~Filters 2~~-~~–4. The spectrum ~~form~~from the filters is imaged on ~~the spectrometer slit~~Spectrometer slits 9~~-~~–12~~(10mm×~~ (10 mm × 60 μm) ~~via lens~~through Lenses 5~~-~~–8. ~~And then final~~Final dispersion is achieved by ~~the convex~~Convex grating 17~~-~~–20 after reflection by ~~the concave mirror~~Concave mirrors 13~~-~~–16, ~~that is~~which are used in the first order. ~~Finally the~~The spectrum is imaged onto ~~2-dimensional~~2D (spectral and spatial ~~dimension~~dimensions) CCD detectors 21~~-~~–24.

~~First of the~~The first calibration ~~modes~~mode is ~~the~~ solar calibration~~, the sun~~. The solar spectrum that is observed by this mode is used to perform accurate wavelength calibrations and ~~to~~ normalize the Earth spectra ~~in order~~ to ~~obtained the~~obtain absolute Earth reflectance spectra. ~~The solar~~Solar radiation enters the instrument through a mesh (transmission 10%) by opening the solar aperture mechanism~~,~~ and is diffused by ~~the~~a selected diffuser. Light from the diffusers illuminates the folding mirror~~,~~ and is then reflected to ~~the~~a telescope optical path. The folding mirror in this position blocks the Earth radiance ~~form~~from the primary mirror. The EMI equipped with one surface reflectance aluminum diffuser (40 mm~~×~~ × 16 mm) and one quartz volume diffuser (QVD~~,~~; 40 mm~~×~~ × 16 mm~~×~~ × 6 mm~~) ,~~), which consists of a 6~~-~~ mm thick quartz ground on both sides and is coated with aluminum on the backside. ~~Besides~~ In addition to its use for radiometric calibration, the QVD is used once per day to provide ~~the~~a solar reference spectrum~~, this is~~ because considerably less ~~structure~~structures are introduced by the QVD than the aluminum diffuser [*Ruud Dirksen et al., 2004, Johan de Vries et al., 2005*]. The aluminum diffuser is mainly used for monitoring ~~of~~ optical degradation behavior in space~~, which~~. This monitoring is performed monthly.

The second calibration mode is the white light source (WLS) calibration~~, a~~. A quartz tungsten halogen ~~white light source (~~WLS~~,~~ (6 V, 10 W) is used to ~~monitoring of the~~monitor CCD detector properties. The light ~~form~~from the WLS ~~travel~~travels through the transmission diffuser and is reflected to the telescope optical path.

Large spectral range from 240 nm to 710 nm combined with high spectral resolution(0.3 nm to 0.5 nm) of the EMI enables the measurement of several trace gases(e.g., NO2, O3, SO2, BrO, HCHO) as well as aerosol, see Table 2. To achieve a high retrieval precision, a high SNR is required for the scattered radiance from the UV to the VIS.

Table 2. EMI data products.

Product Name	**Wavelength Band/nm**
O3	300-345(UV1,UV2)
SO2	305-330(UV1,UV2)
NO2	425-500(VIS1)
BrO	344-360(UV2)
HCHO	335-360(UV2)
Aerosol	UV2,VIS1,VIS2

2 Preflight calibration

The EMI detection ~~ability needs matching~~capability must match the changes ~~of~~in the Earth radiance~~,~~ ~~thus~~. Thus, the instrument can obtain ~~better data~~enhanced measurements from in~~-~~-orbit. ~~In order to get the response performance of the instrument, high precision~~High-accuracy spectral and radiometric ~~calibration~~calibrations are required on the ground to obtain the response performance of the instrument [*A. Perez Albinana et al., 2002, Marcel Dobber et al., 2006, B. Ording et al., 2016, Quintus Kleipool~~,~~ et al., 2018*].

2.1 Spectral calibration

~~The~~A spectral calibration is performed in ~~the~~ Earth observation mode (EOM) during laboratory calibration. The calibration results of the EOM can be applied to ~~Solar~~solar calibration mode (SCM~~),~~) (see Section 2.3~~ section.~~). The ~~employed~~utilized tunable laser (OPOTEK: RADIANT) ~~has a~~exhibits output spectrum ~~range~~ranges of 193~~-410nm~~–410 and 410~~-2500nm~~–2500 nm, which can cover 240~~-710nm~~–710 nm of the EMI~~.~~ with the wavelength ~~precision 10pm~~accuracy of 10 pm. In addition, the spectral calibration is ~~carried out~~performed in a clean room, ~~which can reduce~~thereby reducing the influence of temperature and humidity.

The spectral calibration is ~~needed~~required in the spectral and spatial ~~dimension~~dimensions. The tunable laser output wavelength space is ~~5nm~~5 nm for the UV2 channel~~,~~ and ~~is 10nm~~10 nm for the UV1, VIS1, and VIS2 ~~channel calibration~~channels in the spectral dimension. The spectral lines have full widths at half maximum (FWHM) that are typically ~~an~~1 order of magnitude lower than the EMI spectral resolution, thus providing ~~basically~~ delta inputs to the EMI ~~instrument~~ in the wavelength dimension~~, as a result~~. Therefore, the influence of the slit function of the laser is removed. In the spatial dimension, the instrument ~~has to~~must be rotated ~~in~~for 21 steps ~~according to~~in accordance with the ~~5.~~5~~°~~.5 ° interval to cover the full FOV. The spectral calibration and dark background ~~data~~ are recoded.~~–~~

The wavelength calibration of the EMI instrument is ~~given by~~expressed as

$$\lambda_{i,j} = \sum_{m=0}^{N} c_{k,j} \cdot p^k \quad (1)$$

where λ is the wavelength of ~~the~~a pixel, i is the column number~~,~~, j is the row number, and $c_{m,j}$ ~~are~~ is the wavelength calibration polynomial ~~coefficients.~~coefficient. N is the order of the polynomial, which is 3 for the EMI wavelength calibration. The spectral lines of a laser distribute uniformly in the spectral dimension, ~~which ensure the~~ thereby ensuring a polynomial fitting precision. The four channel wavelength ~~calibration~~calibrations of a center ~~field of view~~FOV (CFOV) in the spectral dimension are ~~shown~~depicted in Fig. 2.

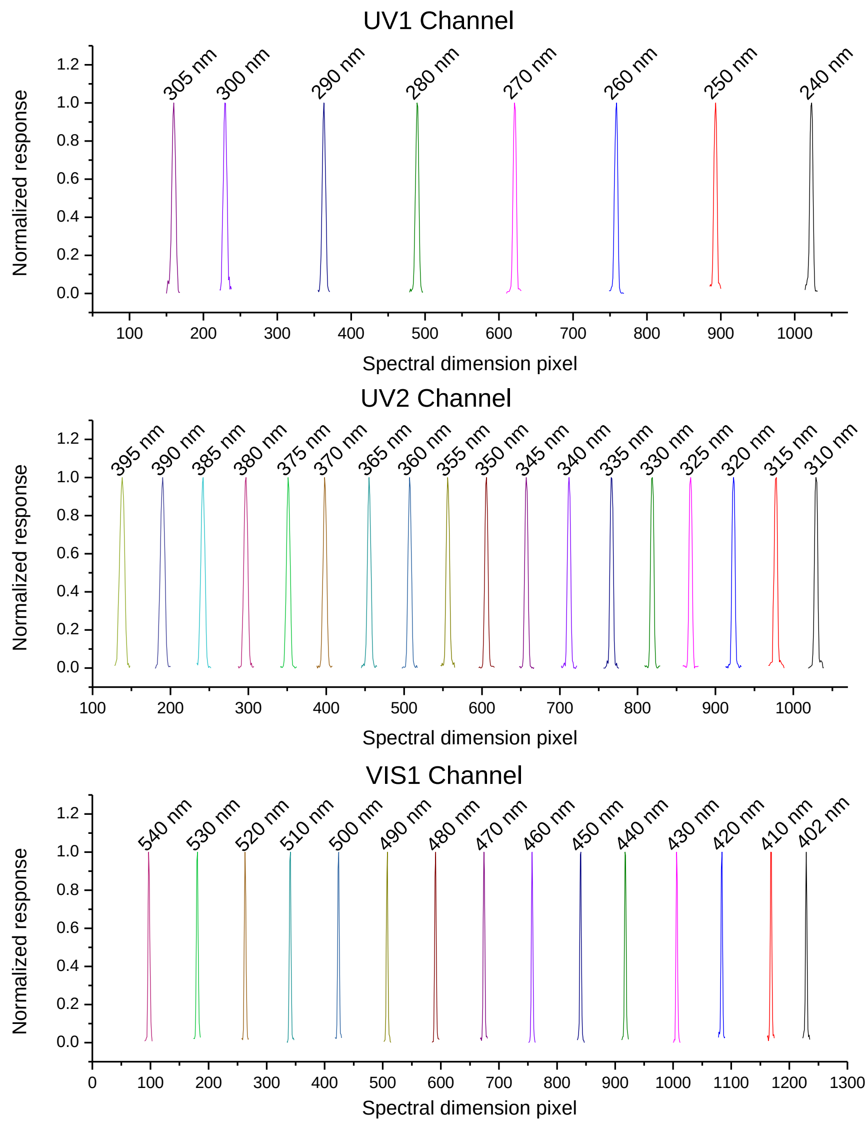

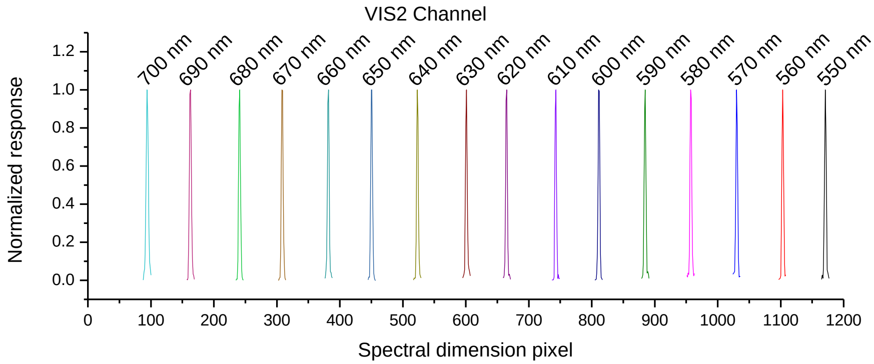

Fig.2. EMI center field of viewCFOV wavelength calibration for each channel. The upper panel presents the UV channel, whereas the lower panel presentsdisplays the VIS channel. The spectral responses are normalized.

The CFOV spectral rangeranges of each channel are shownsummarized in table 2, theTable 3. The spectral range in other field of view areFOVs is discussed lattersubsequently.

Table 23. CFOV spectral rangeranges

Channel	Spectral Range/nm
UV1	236.44～31744–317.28
UV2	306.08～40708–407.12
VIS1	395.50～55250–552.63
VIS2	534.63～71263–712.90

The spectral calibration in the spatial dimension are shownis demonstrated in Fig. 3. It can be seen that the A smile effect in the spatial dimension exists in each channel, and the wavelength position on thea detector array varies with different field of viewFOVs [*P. S. Barry et al., 2002, Robert A et al., 2003, Luis Guanter et al., 2006*]. The wavelength in a marginal field of view shiftFOV shifts to a long wave for the UV channel and shift to a short wave for the VIS channel. Figure 3 exhibits the wavelength (pixel) shifts between the CFOV and the other FOVs.

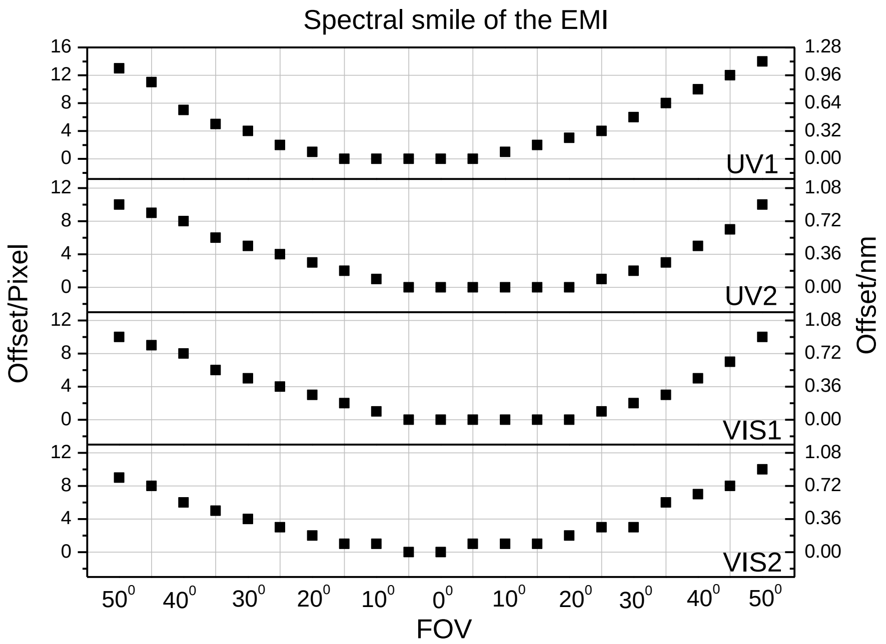

Fig.3. Spectral calibration in the spatial dimension.

The wavelength (pixel) shift enlarges from the CFOV to the edge FOV. The UV1, UV2, VIS1, and VIS2 wavelength (pixel) shifts of the edge FOV are 1.12 nm (14 pixels), 0.9 nm (10 pixels), 1.2 nm (10 pixels), and 1.3 nm (10 pixels), correspondingly. For the L1b processor of the EMI, the spectral smile effect will be calibrated using a spectrum-matching technique.

The spectral response of the EMI can be considered as ~~the~~a Gaussian-type function~~, its~~. The FWHM~~(full width at half maximum)~~ of an instrumental line shape (ILS) function is known as the spectral resolution of the spectrometer channels. The FWHM of the ~~EMI~~ILS by Gaussian fitting is ~~shown~~displayed in ~~table 3.~~Table ~~3~~4.

Table 4. FWHM of the ILS

FOV	UV1/nm	UV2/nm	VIS1/nm	VIS2/nm
50 °	*0.44*	*0.45*	*0.34*	*0.49*
40 °	*0.39*	*0.39*	*0.29*	*0.39*
30 °	*0.40*	*0.38*	*0.29*	*0.40*
20 °	*0.42*	*0.43*	*0.31*	*0.39*
10 °	*0.42*	*0.47*	*0.33*	*0.39*
0 °	*0.43*	*0.49*	*0.34*	*0.40*
10 °	*0.41*	*0.46*	*0.34*	*0.38*
20 °	*0.38*	*0.41*	*0.32*	*0.34*
30 °	*0.36*	*0.36*	*0.34*	*0.30*
40 °	*0.38*	*0.36*	*0.38*	*0.28*

50 °	*0.45*	*0.43*	*0.48*	*0.34*

The overall accuracy of the spectral calibration is determined by three ~~mayor~~major factors~~, firstly by~~ as follows: (1) the accuracy of a laser output wavelength, which is ~~better~~less than 0.~~01nm, secondly by~~01 nm; (2) the ~~stability~~accuracy of the EMI spectral response, which is determined by 20 spectral response ~~data~~measurements from the same laser output line (<0.~~014nm), thirdly by~~014 nm); (3) a fitting method (using ~~the~~ least ~~square~~squares method~~), the~~). The accuracy of the polynomial fitting is ~~about~~approximately 0.~~040nm~~040 nm, and the Gaussian fitting is ~~about~~approximately 0.~~020nm~~020 nm. The final accuracy of the wavelength calibration is ~~better~~less than 0.~~05nm~~05 nm, and the ~~spectral response function~~accuracy FWHM of the ILS is ~~better~~less than 0.~~03nm~~03 nm.

2.2 Thermal vacuum test

The spectral calibration discussed ~~above~~previously is performed in an atmospheric environment, which can provide detailed spectral response characteristics. ~~In order~~A thermal vacuum test is performed (Fig. 4) to ~~obtain~~determine the difference between the atmospheric and vacuum ~~environment~~environments and ~~to~~ obtain the spectral response characteristics ~~in~~under thermal vacuum conditions (EMI in-flight conditions~~), the thermal-vacuum test is performed, see Fig.4~~). A mercury argon lamp is used as light source for EMI. The EMI ~~instrument~~ views ~~the~~a mercury argon lamp through ~~the~~a thermal~~-~~ vacuum chamber window. ~~Because~~Owing to the ~~limit~~limitations of ~~a~~the rotational device and ~~the~~ window size, the ~~center field of view of EMI~~EMI CFOV is measured in the thermal~~-~~ vacuum chamber.

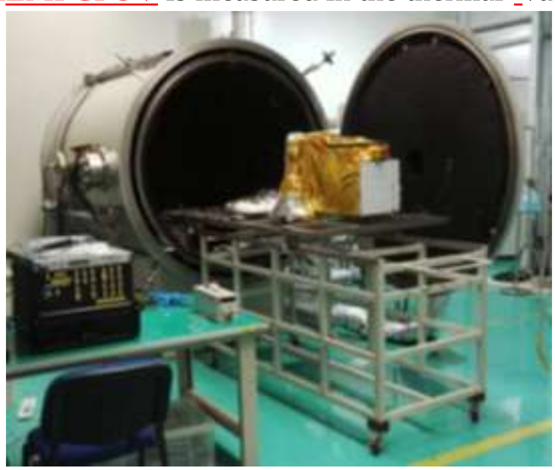

Fig.4. Thermal vacuum test of the EMI.

The thermal vacuum conditions include pressure, optical bench temperature, and CCD temperature~~:~~.

Pressure:

AE: Atmospheric Environment

PV~~-~~: Pumping Vacuum

NFP: Nitrogen Filling Process

Optical bench temperature

LT: Low Temperature~~(276K~~ (276 K)

HT1: High ~~Temperature1(290K~~Temperature 1 (290 K)

HT2: High ~~Temperature2(288K~~Temperature 2 (288 K)

HT3: High ~~Temperature3(299K~~Temperature 3 (299 K)

MT1: Middle ~~Temperature1~~Temperature 1 (284K)

MT2: Middle ~~Temperature2~~Temperature 2 (283K)

MT3: Middle ~~Temperature3~~Temperature 3 (285K)

NTC: No Temperature control

CCD temperature:

UV1, UV2: ~~254K~~254 K

VIS1, VIS2: ~~No~~The temperature ~~control~~is the same as that of the optical bench.

The wavelength shift and FWHM ~~variety~~of the ILS in different conditions ~~is~~are analyzed.

The pixel position ~~corresponding~~that corresponds to the emission peak of the mercury argon lamp is obtained by ~~Gaussians~~Gaussian fitting. The wavelength shifts of the four channels are ~~shown~~displayed in Fig. 5.

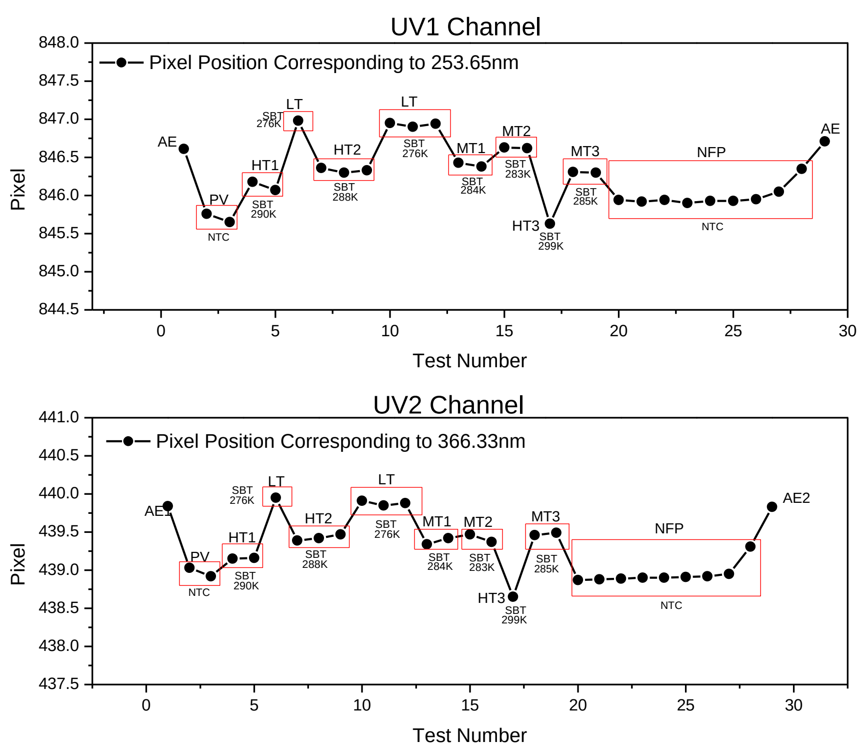

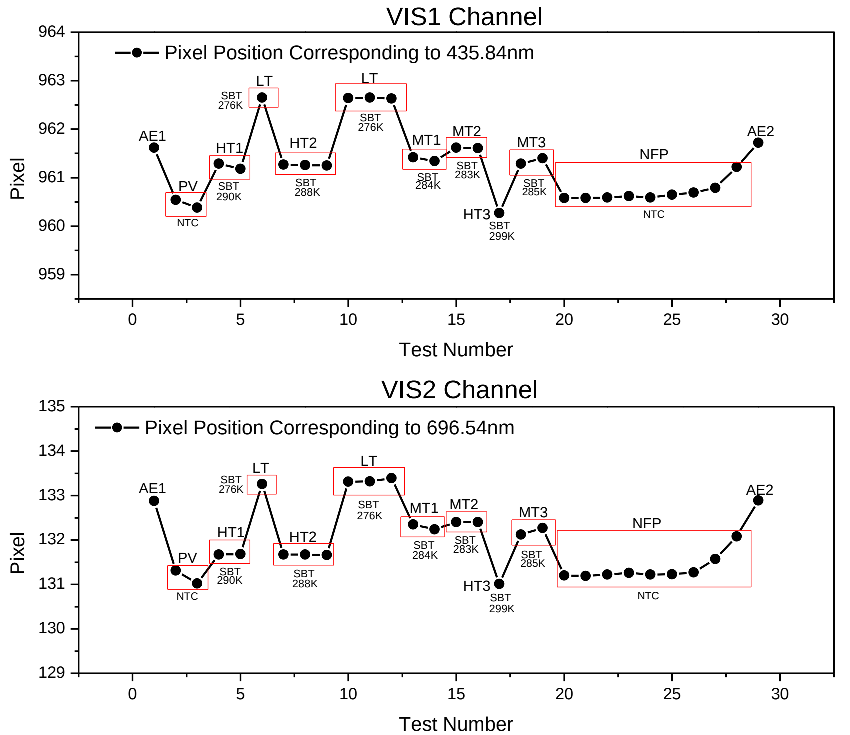

Fig.5. Wavelength shifts from the atmospheric environment to vacuum: UV1/0.~~8pixel(about~~8 pixel (approximately 0.~~06nm~~06 nm), UV2/0.~~8pixel(about~~8 pixel (approximately 0.~~07nm~~07 nm), VIS1/~~1pixel(about~~1 pixel (approximately 0.~~1nm~~1 nm), VIS2/1.~~5pixel(about~~5 pixel (approximately 0.~~2nm~~2 nm); Wavelength shifts from HT1 to LT in vacuum: UV1~~:/1pixel(about~~/1 pixel (approximately 0.~~1nm~~1 nm), UV2/~~1pixel(about~~1 pixel (approximately 0.~~1nm~~1 nm), VIS1/1.~~5pixel(about~~5 pixel (approximately 0.~~2nm~~2 nm), VIS2/1.~~5pixel(about~~5 pixel (approximately 0.~~2nm~~2 nm)

The wavelength shifts $\Delta\lambda$ are determined by

$$\Delta\lambda = \lambda_{Vac} - \lambda_{At} = (1-1/n)\lambda_{Vac} \qquad (2)$$

where λ_{Vac} and λ_{At} ~~is~~are the ~~wavelength~~wavelengths in the thermal~~-~~ vacuum chamber and atmospheric environment~~, as~~. The atmospheric refractivity $n>1$ because the thermal~~-~~ vacuum chamber pressure is ~~smaller~~lower than ~~atmospheric pressure,~~ the atmospheric ~~refractivity $n>1$.~~pressure. The wavelength ~~shift~~shifts to a long wave with the decrease ~~of~~in pressure (n becomes ~~larger~~large) and to short wave with the increase ~~of~~in pressure (n becomes ~~smaller~~small) in the thermal~~-~~ vacuum chamber (see PV~~,~~ and NFP results). ~~And~~Furthermore, the wavelength shifts ~~become larger~~enlarge with the increase ~~of~~in λ_{Vac}~~, the~~. The results show that the ~~shift is~~shifts are 0.~~06nm~~06 nm for 253.~~625nm~~625 nm and ~~is~~ 0.~~2nm~~2 nm for 696.~~54nm~~54 nm.

~~From the~~These results~~, it~~ also ~~can be seen~~indicate that the wavelength shifts change with the optical bench temperature ~~in~~under a vacuum condition. The wavelength ~~shift~~shifts to a long wave with the increase ~~of~~in the optical bench temperature and to a short wave with the decrease ~~of~~in the optical bench temperature. The wavelength shift is ~~about~~approximately 0.~~1nm~~1 nm for UV1~~,~~ and UV2 and is ~~about~~approximately 0.~~2nm~~2 nm for VIS1 and VIS2.

The FWHM of the ILS of four channels are ~~shown~~presented in Fig. 6.

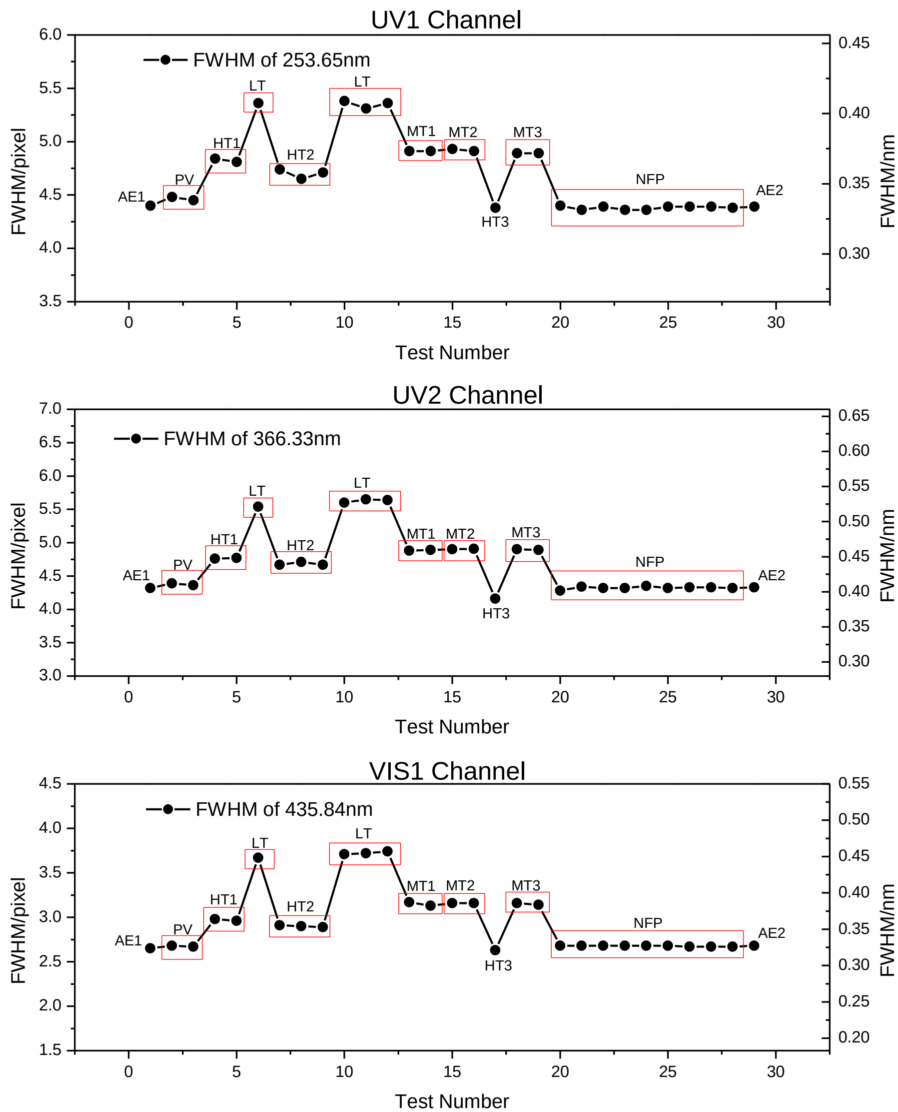

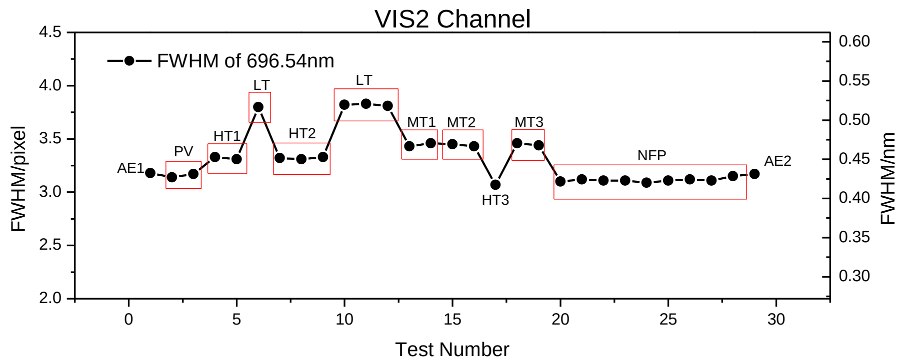

Fig.6. ~~The FWHM results~~Results of the thermal~~-~~ vacuum test on the FWHM of the ILS. The results show that~~,~~ (1) the FWHM of the ILS is ~~basically~~essentially the same in different ~~pressure~~pressures in the thermal~~-~~ vacuum chamber (see AE, PV, and NFP results~~).~~); (2) the FWHM ~~become smaller~~of the ILS shrinks with the increase ~~of~~in the optical bench temperature ~~in~~under a vacuum condition.

The FWHM of the ILS changes with the optical bench temperature ~~see table 4.~~(Table ~~4~~5).

Table 5. FWHM of the ILS changes with optical bench temperature

FWHM of the ILS	**Optical bench temperature/K**						
	276	**283**	**284**	**285**	**288**	**290**	**299**
UV1/~~-~~nm	*0.41*	*0.37*	*0.37*	*0.37*	*0.36*	*0.36*	*0.33*
UV2/~~-~~nm	*0.52*	*0.46*	*0.46*	*0.46*	*0.45*	*0.45*	*0.39*
VIS1/~~-~~nm	*0.45*	*0.39*	*0.39*	*0.39*	*0.36*	*0.36*	*0.32*
VIS2/~~-~~nm	*0.52*	*0.47*	*0.47*	*0.47*	*0.45*	*0.45*	*0.42*

~~From the table 4~~In Table 5, the optical bench temperature ~~has a significant influence on~~significantly influences the spectral resolution of the EMI. For example, the relative deviation of the spectral resolution between the optical bench ~~temperature 276K~~temperatures of 276 and ~~299K~~299 K is up to 25%. Therefore, the in-orbit optical bench temperature of the EMI can be set up ~~according to~~in accordance with the FWHM of the ILS results of the thermal~~-~~ vacuum test.

2.3 Spectral calibration in ~~Solar~~the solar calibration mode

~~Spectral~~The spectral calibration in the ~~Earth observation mode~~EOM is introduced ~~above~~previously. The calibration ~~data~~ in the ~~Sun calibration mode~~SCM shows that the same ~~calibration~~ results are obtained compared with the ~~Earth observation mode~~EOM. We also ~~get~~obtain the solar spectrum from both ~~mode~~modes on the ground~~, a~~. An optical fiber and a small telescope are used to introduce ~~the~~ direct sunlight to the Earth and ~~Sun port~~solar ports. The solar spectrum ~~in~~at the CFOV of the EMI (except ~~the~~ UV1~~) are shown in Fig.7, as~~ because the wavelength range in this channel is not visible on the ground) is illustrated in Fig. 7.

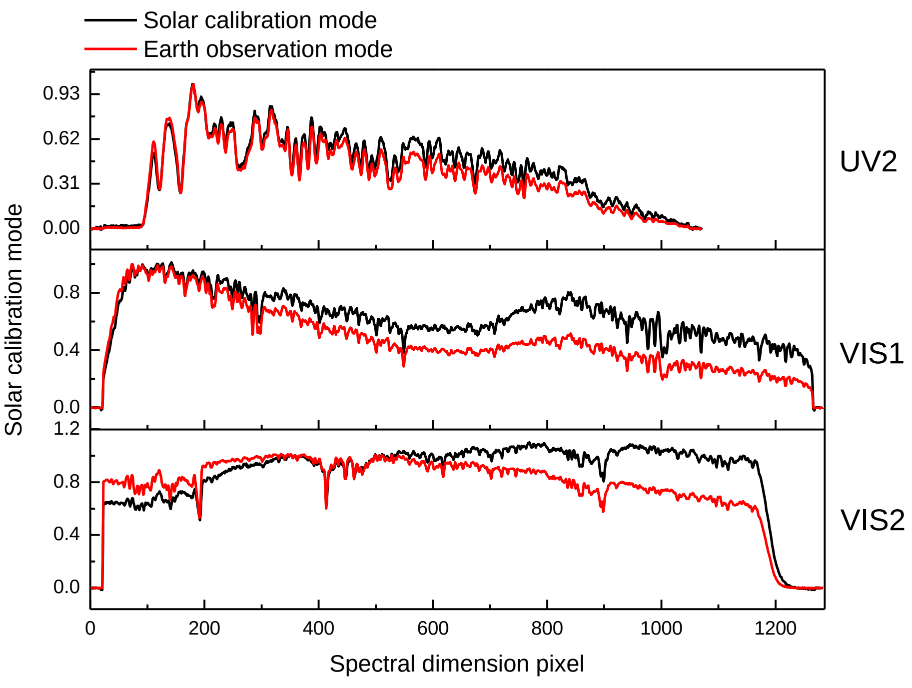

Fig.7. ~~The solar~~Solar spectrum obtained by the EMI on the ground. The aluminum diffuser is used to observe the solar spectrum in the ~~solar calibration mode(see~~ SCM (Fig. 1).

~~From~~In Fig.~~7, it can be seen that~~ 7, the pixel corresponds to the same wavelength in the two ~~mode~~modes. The difference between the spectral shapes is due to the aluminum ~~diffuser's~~diffuser's spectral characteristics, such as hemispheric reflectance and ~~Bi-directional Reflectance Distribution Function (BRDF)[~~ bidirectional reflectance distribution function [*F. E. Nicodemus~~,~~ et al., 1977, Kenneth J. Voss et al., 2000, Xuemin Jin et al., 2009*]. In addition, the spectral features of the aluminum diffuser are introduced to the solar spectrum. The irradiance calibration of the ~~Sun via~~sun through a space-borne diffuser is discussed ~~latter~~subsequently.

3 Radiometric calibration

Radiometric calibration is ~~carried out~~performed in the ~~Earth observation~~EOM and ~~Solar calibration modes~~SCM on the ground. ~~In order to fulfill the requirements of in-orbit observation, several~~Several operating parameters~~ are designed for the EMI instrument~~, such as three ~~different integral~~integration times~~(~~ (i.e., 0.~~5s, 1s , 2s~~5, 1, and 2 s) and 64 ~~different~~ gain ~~values(~~steps (i.e., 0~–63 with an interval of 1~~)~~ ~~corresponding to magnification of 0~5.8~~), are designed for the EMI to fulfill the requirements of an in-orbit observation. The radiometric calibration is performed at different ~~integral~~integration times, and the relationship between gain steps and gain values~~ and magnification~~ is measured.

3.1 Radiometric calibration system

Integrating sphere and ~~diffuse~~diffuser plate radiometric calibration ~~system~~systems are used for the EMI

~~instrument~~. The integrating sphere system with a tungsten halogen lamp is for the radiometric calibration of the UV2, VIS1, and VIS2 ~~channel. And~~channels. Furthermore, the ~~diffuse~~diffuser plate with a ~~1000W~~1000 W xenon lamp (Newport Xenon-6269) is for the UV1 channel (240~~~315nm~~–315 nm), which produces a sufficient ~~ultraviolet~~UV output. The radiance of the radiometric calibration system is monitored by a spectral radiometer~~:~~, that is, Ocean Optics MAYP11868 (200~~~650nm~~–650 nm) for ~~diffuse~~diffuser plate system and USB2000 (200~~~800nm~~–800 nm) for the integrating sphere system. ~~Because it is not possible to illuminate~~The EMI must rotate to complete the radiometric calibration because illuminating the entire 114° instantaneously by the calibration system~~, the EMI instrument needs to rotate to complete the radiometric calibration~~ is infeasible.

The accuracy of the radiance directly determines the EMI radiometric calibration ~~precision~~results. Therefore, the spectral radiometers ~~are~~must also ~~needed to~~ be calibrated~~ carefully. For this reason, the~~. Thus, an NIST-calibrated deuterium lamp (Newport) and a 1000~~-~~-W FEL quartz tungsten halogen lamp (OSRAM) are ~~chosen~~selected to calibrate MAYP11868 and USB2000, separately. ~~During calibration the lamp~~The lamps illuminate a stand diffuser plate, which ~~convert~~converts the lamp irradiance to radiance to calibrate the spectral radiometer, during calibration. The calibrated accuracy of the spectral radiometer is determined by three ~~number of~~ factors~~: the~~ as follows: (1) accuracy of the lamp irradiance standard, ~~the~~(2) accuracy of converting irradiance to radiance, and ~~the~~(3) response accuracy of the spectral radiometer~~, which~~. These factors are discussed in detail below.

The accuracy of the lamp irradiance is traced to the NIST: the deuterium lamp irradiance at ~~50cm~~50 cm is 3.16% in 210~~~350nm,~~–350 nm, and the FEL quartz tungsten halogen lamp ~~irradiance~~irradiances at ~~50cm is~~50 cm are 3.00~~%~~~%–2.40% in 250~~~400nm~~–400 nm and 2.40~~%~~~%–1.60% in 400~~~800nm~~–800 nm.

The method ~~of~~for converting irradiance to radiance is ~~given by~~expressed as

$$L_{rad} = E_{lamp-irrad} \cdot \left(\frac{l_{lamp-plate}}{l_{50cm}}\right)^2 \cdot BRDF_{std-plate} \qquad (3)$$

where L_{rad} is the radiance ~~converting form~~that is converted from the lamp irradiance $E_{lamp-irrad}$ at $l_{lamp-plate}$, which is ~~50cm~~50 cm for the spectral radiometer calibration, that is, $l_{50cm} = 50cm$ ~~;~~; and the stand diffuser plate $BRDF_{std-plate}$ is close to $\frac{1}{\pi}(sr^{-1})$, with the accuracy of 1.25%. The distance between the stand diffuser plate and the lamp is 500 ±~~1mm.~~1 mm.

~~A~~An optical fiber and a small telescope are used by spectral radiometer to observe the stand diffuser plate at an angle of 40°. ~~One hundred observed data is~~A total of 100 measurements were obtained by the spectral radiometer~~, the~~. The accuracy of MAYP11868 response ~~stability~~ is ~~better~~less than 0.80~~%, and the~~%. The accuracy of USB2000 response ~~stability~~ is ~~better~~less than 0.50%. In practice, the radiance monitored by the spectral radiometer is usually different from the radiance of the diffuser plate~~, therefore~~. Therefore, the spectral radiometer needs to work in the linear response region. Five different radiance levels are observed by the spectral radiometer to determine the accuracy of the response linearity~~, the results show that the~~. The accuracy of MAYP11868 response linearity is ~~better~~less than 1.20%, and the accuracy of USB2000 response linearity is ~~better~~less than 1.10%.

Table ~~5~~6. Calibrated accuracy of the spectral radiometer

Uncertainty/%	**MAYP11868 (210nm~~∼~~-350nm)**	**USB2000 (250nm~~∼~~-400nm/400nm~~∼~~-800nm)**
Lamp irradiance standard	*3.16*	*3.00~~∼~~-2.40/2.40~~∼~~-1.60*
Converting (Irradiance to radiance)	*1.27*	*1.27*
Spectral radiometer	*1.44*	*1.21*
Total	*3.70*	*3.48~~∼~~-3.00/3.00~~%∼~~%-2.38*

For the ~~diffuse~~diffuser plate radiometric calibration system, 1000W xenon lamp ~~illuminate~~illuminates the same stand ~~diffuse~~diffuser plate discussed above to produce a near~~-~~-uniform surface light source, which is also produced at the integrating sphere opening by introducing the halogen tungsten lamp light to the sphere ~~via~~through a round pipe. The two radiometric calibration systems have their own highly stabilized power supply. ~~The accuracy of surface light source includes the surface uniformity and stability.~~ The radiometric accuracy of the calibration system is shown in ~~table 6~~Table 7.

Table ~~6~~7. Radiometric accuracy of the calibration system

Uncertainty/%	**Diffuse plate system (210nm~~∼~~-350nm)**	**Integrating sphere (250nm~~∼~~-400nm/400nm~~∼~~-800nm)**
Surface ~~uniformity~~light source	*< 2.00*	*< 2.00*
Spectral radiometer	*3.70*	*3.48~~∼~~-3.00/3.00~~∼~~-2.38*
Total	*< 4.21*	*< 4.02~~∼~~-3.61/3.61~~∼~~-3.11*

3.2 Radiance calibration

The data N_{signal} collected by EMI including dark signal N_{dark} and light signal N_{light} is given by the following:

$$N_{signal} = N_{dark} + N_{light} \qquad (4)$$

where $N_{dark}, N_{light} \propto T_{time}, G_{gain}$, the ~~integral~~integration time T_{time} can be set ~~as~~to 0.~~5s, 1s , 2s~~5, 1, and 2 s, the gain steps G_{gain} can be set ~~form~~from 0 to 63 with the interval of 1.

~~In order to~~To obtain an approximate dark correction and to widely remove the dark-current-induced spectral structures, the mean dark spectra is subtracted [*Birgre Bohn et al., 2017*]. The dark ~~signal~~ and light ~~signal~~signals are discussed separately below.

Dark signal

~~EV2~~The e2v-CCD4720 and ~~EV2~~e2v-CCD5530 are adopted for the UV and VIS channel separately. As the weak ~~ultraviolet~~UV band of the atmospheric light, the two UV channel CCDs are cooled to ~~-~~−20~~℃~~ ℃ to reduce the dark signal. The CCDs for the visible channels do not have independent temperature control, but they work in a constant temperature environment. The temperature is similar to that in the spectrometer, which has temperature control. Thus, the change of CCD temperature is not a problem.

~~The dark~~Dark signal ~~for each pixel is composed of an~~ is obtained when no photons enter the instrument is to add the bias value (electronic offset) N_{bias} and the dark~~ noise~~-current $N_{current}$ multiplied by the integration time t_{inte}.

$$N_{dark} = N_{bias} + N_{current} \cdot t_{inte} \quad (5)$$

The read-out register within the CCD has an excess of 16 blank pixels, which can be used to measure the electronic offset ~~is fairly const, but dark noise~~ on the ground. The measurements show that the offset is not constant but drifts with time (about 0.5% /min). Therefore, the electronic offset is obtained per measurement frame in-orbit, and the electronic offset correction is implemented in the L1b data processor. The dark-current signal is a thermally induced dark-current ~~signal increasing~~that increases with temperature and integration time [*Evelyn Jakel et al., 2007*]. Therefore, a dark signal measurement should be conducted frequently to update the dark data. The dark signal under different ~~integral time~~ integration times is shown in ~~fig.5, which take~~Fig. 5 with UV2 ~~channel and VIS1channel for example~~and VIS1 channels as examples.

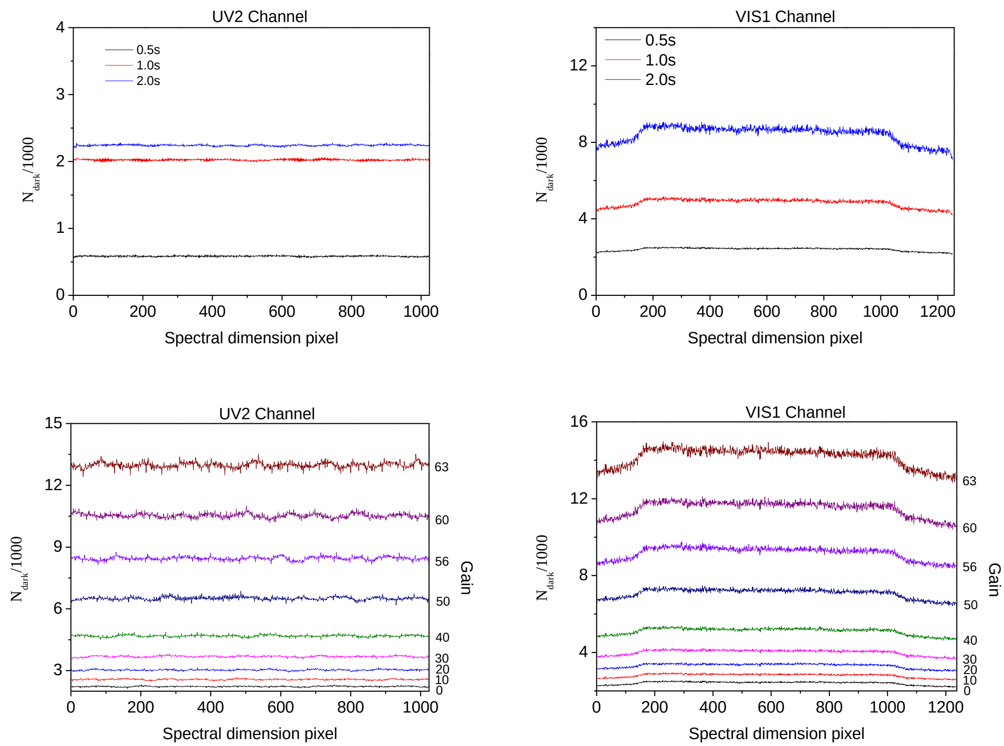

Fig.8. ~~Top: Dark signal under different integral time. Bottom: Dark signal under different gain. The gain is set to 0,10,20,30,40,50,56,60,63~~Top: Dark signal for different integration time. Bottom: Dark signal under different gain steps. The gain steps are set to 0, 10, 20, 30, 40, 50, 56, 60, and 63. The pixels in the readout register cannot be used to accomplish the binning due to the full well limitation. In this case, the pixel binning is accomplished in the Field Programming Gate Array. Fast readout frequency is needed for the process. The fast readout frequency leads to signal distortion. Therefore, the difference between the measurements with 0.5 and 1.0 s integration times is not half of the difference between the measurements with 1.0 and 2.0 s integration times. Based on the signal distortion, we have obtained absolute radiance calibration key data at different integration time on the ground. The calibration key data are used for the L1b data processor.

~~From~~In Fig. 8, the small spectral structure in dark signal is caused by dark noise, which could influence the measured data, especially under weak-light conditions. The dark noise can be ~~get~~obtained by deriving standard deviations of repeated dark measurements~~,~~ and can be reduced by averaging the repeated dark~~ data~~. The dark spectra ~~is~~are recorded for each orbit when EMI is in orbit, and then, the dark spectra under the same ~~work~~working conditions are averaged to correct the observation spectra.

Light signal

The ~~output radiance level of the~~ radiometric calibration ~~system is determined by the xenon lamp output power for diffuse plate system, and is determined by the introduction of the light for integrating~~

~~sphere system~~systems can provide different output-radiance levels. For UV1 channel, the EMI instrument views the standard ~~diffuse~~diffuser plate at an angle of 45.0 ° and at a distance of 50.~~0cm, about~~0 cm. Approximately 13 ° viewing angle of EMI can be illuminated once~~, so~~. Thus, the instrument has to be ~~rotate~~rotated in ~~9~~nine steps to complete the entire 114 °. For the UV2, VIS1, and VIS2 channels, EMI views the integrating sphere opening at a distance of 40.~~0cm, about~~0 cm, and approximately 11 ° can be illuminated once~~, and~~. A total of 11 steps are ~~needed~~required to complete the radiance calibration.

The dark signal is firstly deducted from the radiance calibration data~~ firstly~~. One radiance level of the radiance calibration systems and the corresponding response of the EMI instrument are shown in Fig. 9.

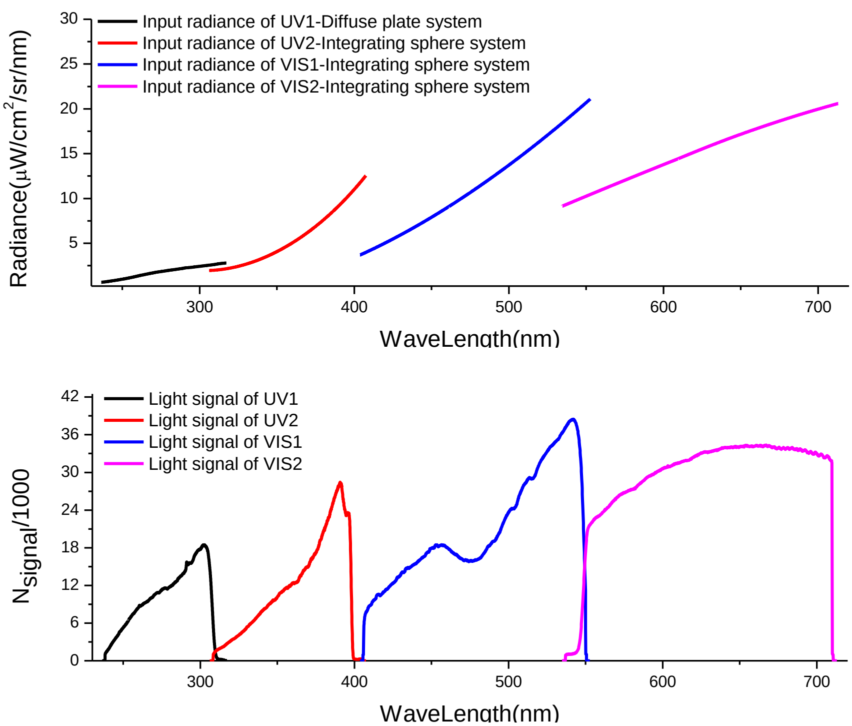

Fig.9. ~~The upper~~Upper panel presents one radiance level of ~~diffuse~~the diffuser plate and integrating sphere system. The lower panel presents the EMI response to the radiance~~, the~~ at integration times 2s (UV1), 1s (UV2, VIS1, VIS2), and at gain step 0. The dark signal is subtracted from the response~~.The work parameters of UV1, UV2, VIS1, VIS2 are : the integral time 2s,1s,1s,1s, and gain 0, 0, 0, 0.~~

~~From Fig.9, there is~~Figure 9 illustrates an overlap band at each end of the channels, which is due to the optical features of the color separation filters. In addition, the response in the wavelength range 460~~~480nm~~–480 nm of VIS1 channel ~~become lower~~lowered, because a filter of this range is placed in front of ~~the slit~~Slit 11~~, the purpose is~~ to ~~make sure~~ensure that the detectors are ~~not saturated~~unsaturated in the case of clouds.

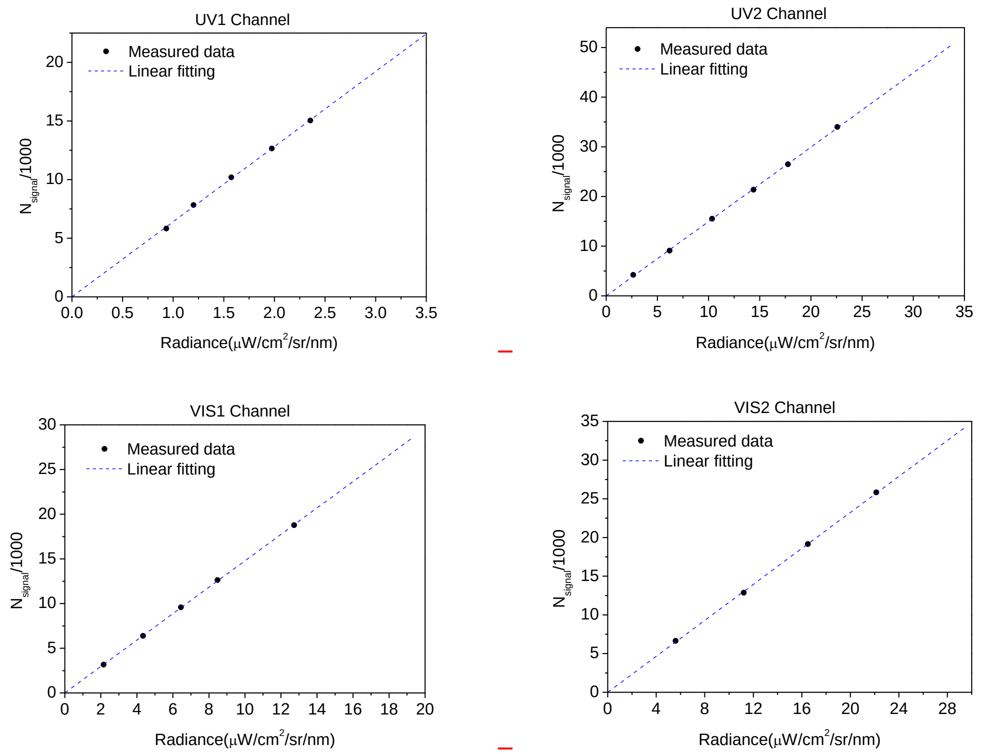

Fig.10. Linear response of the EMI, the signal is corrected by the dark signal. ~~Note that, there is the~~A non-linear response region ~~in the~~exists under very low light signal (equal to the dark signal) condition and high light signal (saturation light signal) ~~conditions~~condition. The ~~integral~~integration time, CCD readout, and gain steps are set up to ensure that the EMI works in the linear response region.

Base ~~on~~ the linear response of the EMI, the radiance calibration model is as follows:

$$L_{radiance} = \alpha \cdot N_{Light} \quad (6)$$

where $L_{radiance}$ is the radiance at the EMI entrance pupil, and α is the radiance response coefficient.

The theoretical relation between gain steps f_{gain} and ~~magnification~~gain value f_{magn} is determined ~~by~~using the following equation:

$$f_{magn} = \frac{5.8}{1 + 4.8 \cdot (63 - f_{gain}) / 63} \quad (7)$$

The light signal under different gain steps is ~~shown~~exhibited in ~~fig.~~Fig. 11, which ~~take~~uses the UV2 and ~~VIS1channel for example~~VIS1 channels as examples.

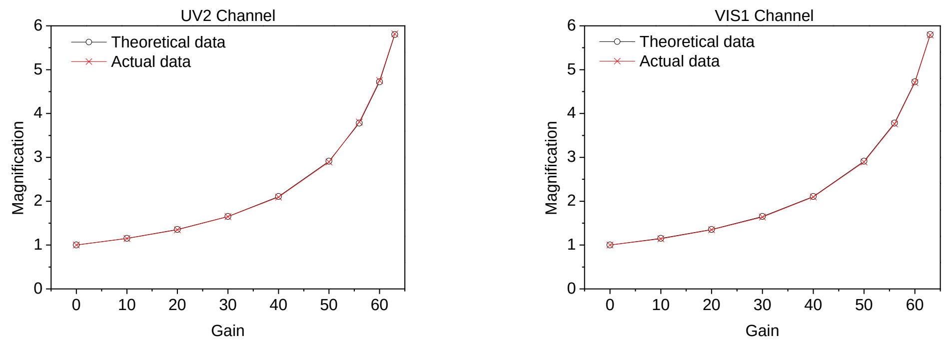

Fig.11. ~~The relation~~Relation between gain steps and ~~magnification, the results show that the~~ gain value are presented. The relative deviation between theoretical and actual data is ~~better~~less than 1.0%. In application, the ~~magnification~~gain value can be obtained from the theoretical relation.

The overall accuracy of the radiance calibration is mainly determined by the accuracy of the radiance calibration system, by the response non-linearity, and by the accuracy of response ~~non-stability~~ of the EMI. The accuracy of the diffuser plate system and integrating system is shown in ~~table~~the Table 7. The response non-linearity can be calculated by the data in Fig. 8, and the results are as follows: 1.13~~%(~~% (UV1), 1.04~~%(~~% (UV2), 1.07~~%(~~% (VIS1~~)~~), and 1.00~~%(~~% (VIS2). The response ~~non-stability~~ accuracy is obtained by 1000 repeated spectra of the EMI, and the results are 1.21~~%(~~% (UV1), 1.26~~%(~~% (UV2), 1.12~~%(~~% (VIS1~~)~~), and 1.14~~%(~~% (VIS2). The accuracy of the conversion of different ~~gains~~gain steps should be ~~consider~~considered in the case of the light signal corrected by the gain value. The final accuracy of the radiance calibration is ~~shown~~summarized in ~~table 7~~Table 8.

~~Table7~~Table8. Radiance calibration accuracy

Channel	Accuracy(%)	
	No gain value corrected	**Gain value corrected**
UV1	*4.53*	*4.64*
UV2	*4.52*	*4.63*
VIS1	*4.31*	*4.43*
VIS2	*4.30*	*4.42*

The pre-flight, radiometric calibration of EMI was not conducted under flight-like vacuum and possibly under thermal conditions due to the limitation of the calibration facility. The EMI on-ground response to the quartz tungsten halogen WLS (6 V, 10 W) is displayed in Fig. 12, which uses UV2 and VIS1 as examples.

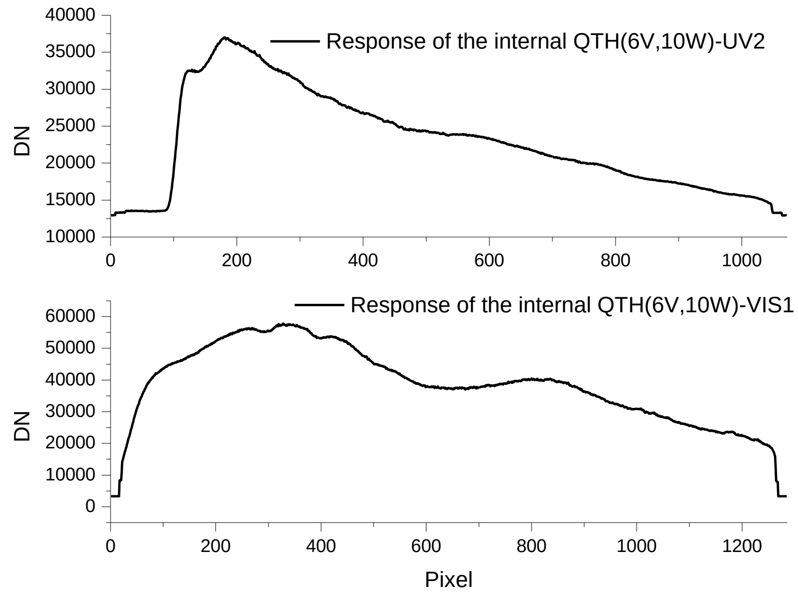

Fig.12. EMI on-ground response to the quartz tungsten halogen WLS

The EMI in-orbit response to the quartz tungsten halogen will be obtained after the launch. The change between the on-ground and in-orbit responses is used to correct the preflight radiometric calibration, which in turn is used to accomplish the in-flight absolute radiometric calibration of the flight data.

3.3 Irradiance calibration

The solar irradiance is calibrated mostly ~~via~~through the onboard diffusers [*S.Noel et al., 2006, Xiaoxiong Xiong et al., 2009*]. The irradiance calibration depends on the incident angles on the onboard diffusers of the EMI. The azimuth angle varies slowly throughout the year from about 16 ° to 28 ° around the nominal value of 22 °~~, the~~. The elevation angle varies from +4 ° to ~~-~~–4 ° around the nominal value of 11 °. The elevation angle change originates from the satellite orbital movement. ~~About~~Approximately 75 images are obtained during a solar observation sequence of ~~150s~~150 s, and each individual image ~~needs to~~must be corrected for ~~the~~ radiometric goniometry.

$$DN_{\alpha_0,\beta_0} = DN_{\alpha,\beta} \cdot f_{\alpha,\beta} \qquad (8)$$

where DN_{α_0,β_0} is the image at the nominal azimuth angle α_0 and elevation angle β_0, which is corrected from the $DN_{\alpha,\beta}$ with the goniometry correction factor $f_{\alpha,\beta}$. ~~And the~~The corrected images are averaged to improve the SNR. The irradiance calibration model of the EMI is as follows:

$$I_{Sun} = [\frac{1}{n}\sum_{i=1}^{n}(DN_{\alpha,\beta} \cdot f_{\alpha,\beta})_i] \cdot \sigma_{\alpha_0,\beta_0} \qquad (9)$$

where $n = 75$, $\sigma_{\alpha_0,\beta_0}$ is the irradiance response coefficient. The goniometry correction factor and irradiance response coefficient of the EMI are calibrated on the ground. A light source has a beam divergence ~~that is~~ comparable to that of the sun~~, which~~. This light source is rotated to cover the azimuth and elevation angle ranges. The goniometry correction factors are shown in Fig~~-~~. 13, which are by definition 1.00 for the nominal azimuth and elevation angles.

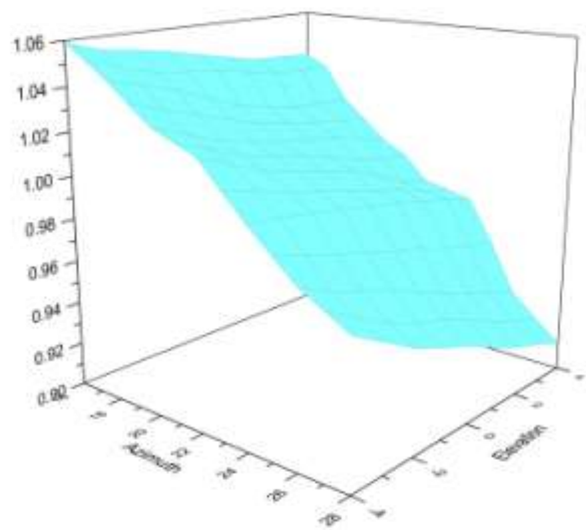

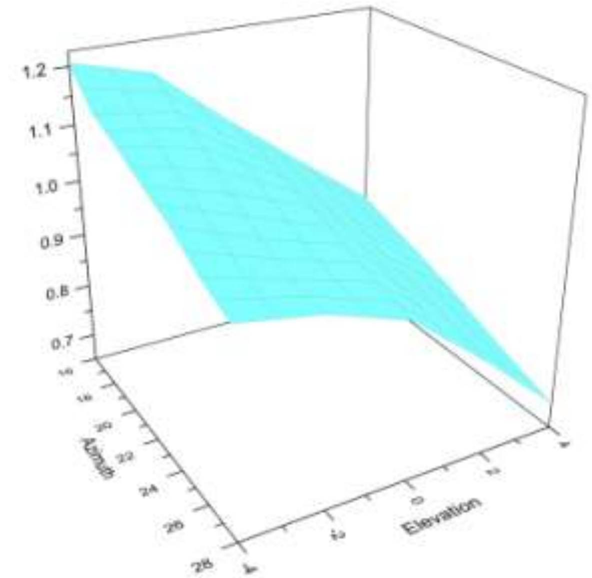

Fig.~~12~~13. Goniometry correction factors for the aluminum diffuser (upper panel) and ~~quartz volume diffuser~~QVD (lower panel) for the ~~center field of view~~CFOV.

The NIST-calibrated 1000W FEL quartz tungsten halogen lamp is used for the absolute irradiance calibration at the nominal azimuth and elevation angles. ~~And the~~The irradiance response coefficient $\sigma_{\alpha_0,\beta_0}$ is obtained for the irradiance calibration model of the EMI.

~~It was found that aluminum~~Aluminum diffusers adopted by the SCIAMACHY project introduce spectral structures in the ~~Sun~~sun reference spectrum [*C.E. Sioris et al., 2004*]. These structures are comparable to trace gas absorption features. They may interfere with DOAS-based retrieval of trace gases~~ hence~~, thereby affecting the accuracy of the retrieved column densities [*A.Richter~~,~~ et al., 2001,2002, Courreges-Lacoste et al., 2004*]. As the QVD ~~introduce~~introduces considerably less structure than the aluminum diffuser, the EMI used it to provide the solar reference spectrum once per day. The aluminum diffuser is mainly used for radiometric calibration purpose, which is performed once ~~monthly~~a month.

~~In addition,~~The EMI works in low Earth orbit (LEO) ~~with the~~at an orbit altitude of 708 km. The critical space environment will affect the performance of materials and components in LEO [*Samuel F. Pellicori,2014*~~]. Such~~], such as atomic oxygen (AO~~)[~~) [*Bruce A. Banks et al., 2008*], ~~Solar~~solar UV, and the energetic protons trapped in the inner Van Allen belt. Space radiation exposure effects on onboard diffusers have been tested and discussed ~~by~~in a previous study [*MinJie Zhao~~,~~ et al., 2015*].

4 Signal-to-noise ratio

The EMI is needed to meet the ~~signal to noise ratio(~~SNR~~)~~ requirements for dark scenes~~(~~, especially in the UV bands~~)[~~ [*Johan de Vries et al., 2009*], to ensure the accuracy of retrieved results. ~~A~~An SNR model is introduced, ~~which~~and it is in good agreement with the experimental result. ~~And the~~The EMI in-orbit

SNR is estimated by using the SNR model and MODTRAN~~.~~ [*A. Berk et al., 1989*]. The SNR estimation for advanced hyperspectral space instrument ~~is~~have been discussed ~~by~~elsewhere[*Andreas Eckardt et al., 2005, Lang Junwei et al., 2013*~~-~~].

The electrons generated by a signal pixel can be calculated by the following:

$$s_e = \frac{\pi}{4}(\frac{D}{f})^2 \cdot \tau(\lambda) \cdot L(\lambda) \frac{A_d t_{int} \lambda}{hc} \eta(\lambda) \Delta\lambda \qquad (10)$$

where D/f is the relative aperture of optics, h is the Plank constant, c is the light speed, $\tau(\lambda)$ is the transmission of optics, $L(\lambda)$ is the sensor input radiance in $\mu W / cm^2 / sr / nm$, $\Delta\lambda$ is the spectral bandwidth of a single spectral line, A_d is the pixel area, t_{int} is the integration time, and $\eta(\lambda)$ is ~~Quantum~~the quantum efficiency of CCD.

The main part of the total noise is the shot/photon noise generated by the incident radiation. The shot/photon noise can be described by the Poisson distribution, and can be calculated as follows:

$$\delta_{shot} = \sqrt{s_e} \qquad (11)$$

The other ~~noise~~noises include a dark noise δ_{dark} and ~~read-out~~a readout noise of the CCD δ_{read}. Generally, the SNR can be calculated ~~by~~using the following equation:

$$SNR = \frac{s_e}{\sqrt{\delta_{shot}{}^2 + \delta_{dark}{}^2 + \delta_{read}^2}} \qquad (12)$$

The SNR can be improved by pixel binning,

$$SNR = MS_e / \sqrt{MS_e + M\delta_{dark}{}^2 + \sigma_{read}^2} \qquad (13)$$

where M is the binning factor~~, see table~~ (Table 1~~.~~).

The output digital number of a signal pixel is obtained by the conversion factor f of the CCD:

$$DN = f \cdot S_e \qquad (14)$$

For the SNR model of the EMI, it is impossible to measure the signal and noise separately. ~~In~~ One way to do this in practice~~, one way~~ is to adopt the mean value of the repeat DNs as the signal and to adopt the standard deviation of the repeat DNs as the noise. In this case, N repeated measured spectra of EMI ~~is~~are recorded by observing the uniform-stable light source of the calibration system. ~~And the~~The measured SNR is calculated by the following:

$$SNR = \frac{\overline{DN}}{\sqrt{\frac{\sum_{i}^{N}(DN_i - \overline{DN})^2}{\text{N-1}}}} \qquad (15)$$

The offset is deducted from the DNs. Fig.~~13 show~~ 14 shows the simulation and measured SNR results of VIS1 at the input sensor radiance.

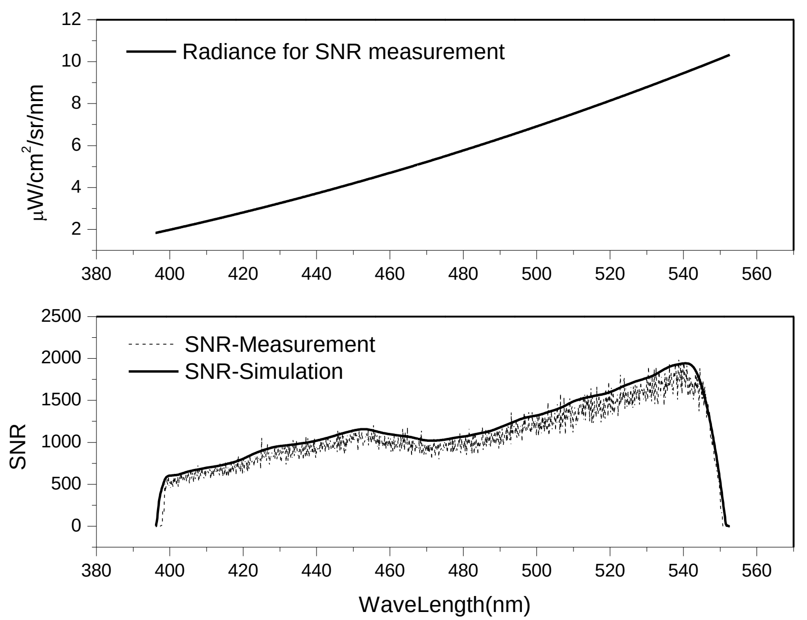

Fig.~~13. The upper~~14. Upper panel presents the radiance of the integrating sphere system for SNR measurement of VIS1 in ~~lab~~the laboratory. The lower panel presents the results of measured SNR (solid line) and simulation result (dotted line) for the radiance of the upper panel~~,~~ with ~~the~~an integration time of ~~2s~~2 s and ~~the~~a binning factor of 4. The measured SNR in the wavelength range 460~~~500nm become lower~~ – 500 nm lowers because a filter of this range is placed in front of the slit 11~~, the purpose is~~ to make sure that the detectors are not saturated in the case of clouds. ~~And there~~There is an overlap band at the end of the channel, which is due to the optical features of the color separation filter. In addition, there are 24 dark pixels at the end of the channel ~~with~~when the measured SNR is ~~about~~approximately zero.

For the measured SNR, 100 repeated measured spectra of EMI ~~is~~are recorded by observing the integrating sphere system with ~~the~~an integration time of ~~2s and the binning factor of 4. The offset signal is deducted from the spectra using the equation?.~~2 s. For the simulation SNR, the F-number of EMI optics $F\# = 3.2$, the spectral width of VIS1 $\Delta\lambda = 0.12nm$, the area of a ~~singl~~single pixel

$A_d = 22.5 \times 22.5(um^2)$, the integration time $t_{int} = 2s$, and the binning factor $M = 4$. ~~Fig show~~ Figure 14 demonstrates that the measured SNR is lower than the simulation SNR~~, the possible reasons are the non-uniformity and non-stability of the light source and the pixel response non-uniformity(PRNU) for the binning pixels. But the results also show that it~~. However, SNR is a good choice ~~to estimate~~for estimating the EMI in-orbit SNR using the SNR model.

The simulation of the EMI in-orbit SNR ~~of~~in the UV2, VIS1, and VIS2 channels are ~~shown~~displayed in Fig. ~~14~~15. The in-orbit SNR of this channel is not estimated as the solar light in the band of ~~the~~channel UV1 (240~~-310nm~~ – 310 nm) is absorbed by the atmosphere.

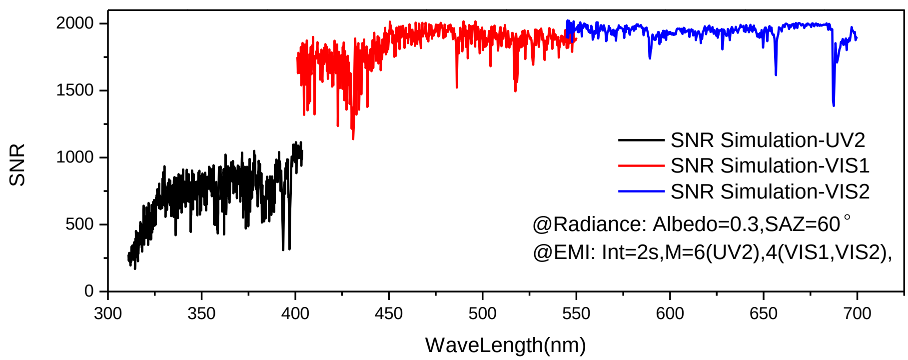

Fig.~~14. The simulation~~15. Simulation EMI in-orbit SNR of UV2, VIS1, and VIS2. The input radiance for the SNR model is obtained by MODTRAN with the albedo of 0.3 and ~~whit~~with the sun zenith ~~of~~at 60°. The EMI simulation SNR ~~with the~~has an integration time of ~~2s, the~~2 s; it has binning ~~factor~~factors of 6 for ~~UV2~~UV 2 channels and 4 for VIS channels~~, the~~. The spectral bandwidth of a pixel ~~of~~was 0.~~09nm~~09 nm for UV2, 0.~~12nm~~12 nm for VIS1, and 0.~~13nm~~13 nm for VIS2.

The EMI in-orbit ~~radiance~~simulation $SNR_{simulation}$ is obtained by ~~MODTRAN for~~ the radiance $R_{simulation}$ at an albedo of 0.3 ~~at 60° sun zenith is used~~and solar zenith of 60°. The in-orbit simulation SNR at the radiance of 1.27/10.89 $\mu W / cm^2 / sr / nm$ can be achieved by the following equation:

$$SNR = SNR_{simulation} \cdot \sqrt{\frac{R}{R_{simulation}}} \qquad (16)$$

where R is 1.27 for UV channels and 10.89 $\mu W / cm^2 / sr / nm$ for VIS channels.

For the in-orbit simulation ~~EMI in-orbit SNR. The in-orbit~~ SNR ~~of~~at the ~~UV2 is about 700,~~radiance of

1.27/10.89 $\mu W / cm^2 / sr / nm$, the ~~VIS1 is about 1800 and the VIS2 is about 2000~~results are presented in Table 9.

Table 9. In-orbit simulation SNR at the requirement radiance

Channel		**SNR (simulation)**	**SNR (requirements)**
UV2	330nm	328	200
	360nm	356	200
	390nm	388	200
VIS1	420nm	1860	1300
	480nm	1900	1300
	540nm	2040	1300
VIS2	560nm	2200	1300
	620nm	2300	1300
	680nm	2400	1300

5 Conclusions

The spectral and radiometric response performance of the EMI is obtained by ~~the~~ preflight calibration. ~~At~~The on-ground calibration results are shown as follows:

Spectral calibration results:

UV1: 236.44–317.28 nm with the spectral resolution ≤0.45 nm;

UV2: 306.08–407.12 nm with the ~~same time~~spectral resolution ≤0.49 nm;

VIS1: 395.50–552.63 nm with the spectral resolution ≤0.48 nm;

VIS2: 534.63–712.90 nm with the spectral resolution ≤0.49 nm;

The final accuracy of the wavelength calibration is <0.05 nm.

Radiometric calibration results:

UV1: 4.64%, UV2: 4.63%, VIS1: 4.43%, VIS2: 4.42%.

The on-ground calibration results meet the performance requirements of the EMI.

Simultaneously, the obtained calibration key data ~~is~~are used for the L1b processor. ~~After launch, the~~The EMI in-orbit performance after the launch may change ~~due to~~given the vibration of the launching and changes in the ~~change of the environment~~environmental conditions. Therefore, the EMI in-orbit calibration is performed ~~in order~~ to verify preflight calibration and ensure calibration accuracy. For the EMI, the in-orbit wavelength calibration is performed by ~~use of~~using the Fraunhofer lines in the ~~sun spectra~~solar and Earth spectra. The in-orbit radiometric calibration is performed by ~~observe~~observing the sun ~~via~~through the onboard diffusers. During the EMI flight, the ~~low Earth~~

~~orbit~~LEO space environment ~~such as atomic oxygen, the~~factors including AO, solar UV, and energetic protons will affect the EMI response performance~~, the aluminum~~. Aluminum diffuser and ~~the~~ quartz tungsten halogen ~~white light source(6V, 10W)~~WLS are used to monitor the ~~disintegration~~degradation of the EMI.

~~**Acknowledgements.**~~

Acknowledgment

This research was supported by ~~grant from~~the National Natural Science Foundation of China (Grant No. 41705016).

References

~~A. Hahne, A. Lefebvre, J. Callies, et al. GOME: A New Instrument for ERS-2. ESA Bulletin, 73(73): 22-29, 1993.~~

A. Berk, L. S. Bernstein and D. C. Robertson, “MODTRAN: A Moderate Resolution Model for LOWTRAN7,” Rpt. No. GL-TR-89-0122, Air Force Geophys. Lab., Bedford, MA 01731, 1-38, 1989.

Andreas Eckardt, Stefan Hofer, Christian Neumann, and Wolfgang skrbek. SNR estimation for advanced hyperspectral space instrument. Infrared Spaceborne Remote Sensing. Proceedings of SPIE, 5883, 588303-1,2005.

A. Perez Albinana and R. Munro. The calibration of GOME-2 data. Infrared Spaceborne Remote Sensing X. Proceedings of SPIE 4818, 185-192, 2002.

A.Richter, T.Wagner.Diffuser plate spectral structures and their influence on GOME slant columns. Technical note, January 2001.

A.Richter, F.Wittrock.GOME MEASUREMENTS OF STRATOSPHERIC AND TROPOSPHERIC BrO. Adv Space Res. 29(11):1667-1672, 2002.

Birgre Bohn and Insa Lohse, Calibration and evaluation of CCD spectroradiometers for ground-based and airborne measurements of spectral actinic flux densities. Atoms. Meas. Tech., 10, 3151-3174, 2017.

B. Ording, A. Ludewig, R. Hoogeveen, D. ten Bloemendal, J. Dingjan, R. Voors, and J. de Vries. RESULTS OF THE TROPOMI CALIBRATION CAMPAIGN. International Conference on Space Optics-ICSO 2016. Proc of SPIE, 10562, 105623B-1, 2016.

Bruce A. Banks, Kim K. de Groh, Sharon K. Miller, and Deborah L. Watters, Lessons Learned From Atomic Oxygen Interaction With Spacecraft Materials in Low Earth Orbit, NASA/TM-2008-215264.

C.E. Sioris, T.P. Kurosu,et al. Stratospheric and tropospheric NO2 observed by SCIAMACHY: first results. Advances in Space Research.34:780-785, 2004.

Courreges-Lacoste, Hedser van Brug, J.Groote Schaarsberg,et al. Spectral Features on reference diffusers: measurements and analysis. SPIE, 5234: 304-313, 2004.

Evelyn Jakel and Manfred Wendisch. A CCD spectroradiometer for ultraviolet actinic radiation measurements. JOURNAL OF ATMOSPHERIC AND OCEANIC TECHNOLOGY, 24, 449-462, 2007.

F. E. Nicodemus, J.C. Richmond, J. J. Hsia, I. W. Ginsberg, and T. Limperis, Geometric Consideration and Nomenclature for Reflectance, National Bureau of Standards, NBS monograph 160 Oct, 1977.

H. BOVENSMANN, J. P. BURROWS, M. BUCHWITZ, J. FRERICK, S. NOËL and V. V. ROZANOV, SCIAMACHY: Mission Objectives and Measurement Modes. JOURNAL OF THE ATMOSPHERIC SCIENCES. 56, 127-150, 1999.

Johan de Vries, Robert Voors, Ruud Dirksen and Marcel Dobber. In-orbit Performance of the Ozone Monitoring Instrument. Sensors, Systems, and Next-Generation Satellites IX. Proc. of SPIE, 5978, 59780T-1, 2005.

Johan de Vries, Robert Voors, Agnes Mika,et al.TROPOMI,the solar backscatter satellite instrument for air quality and climate, heads towards detailed design. SPIE, 7474:747409, 2009.

JOHN P. BURROWS, MARK WEBER, MICHAEL BUCHWITZ, VLADIMIR ROZANOV, ANNETTE LADSTÄTTER- WEI β ENMAYER, ANDREAS RICHTER, RÜDIGER DEBEEK, RICARDA HOOGEN, KLAUS BRAMSTEDT, KAI-UWE EICHMANN and MICHAEL EISINGER, The Global Ozone Monitoring Experiment(GOME): Mission Concept and First Scientific Results, JOURNAL OF THE ATMOSPHERIC SCIENCES. 56, 151-175, 1999.

Kenneth J. Voss, Albert Chapin, Marco Monti and Hao Zhang, Instrument to measure the bidirectional reflectance distribution function of surface, Appl. Opt. 39, 6197-6206, 2000.

Lang Junwei, Wang Yueming and Wang Jianyu. A new SNR Model for Space-borne Hyperspectral Imagers Including Atmospheric Scattering Influence. International Symposium on Photoelectronic Detection and Imaging 2013: Imaging Spectrometer Technologies and Applications. Proc. of SPIE, 8910, 89101l-1, 2013.

Luis Guanter, Rudolf, Jose Moreno. Spectral calibration of hyperspectral imagery using atmospheric absorption features. APPLIED OPTICS. 5(10):2360-2370, 2006.

Marcel Dobber, Ruud Dirksen, Pieternel Levelt, Gijsbertus ban den Oord and Quintus Kleipool, EOS-Aura Ozone Monitoring Instrument in-flight performance and calibration, SPIE, 6296, 62960R-1- 62960R-12, 2006.

Minjie Zhao, Fuqi Si, Cheng Liu, Yihuai Lu, Yu Wang, Shimei Wang, Yi Zeng, Yu Jiang, Haijin Zhou, Wenqing Liu. The effect of AO/UV/RD exposure on space-borne diffusers: A comparative experiment. Appl. Opt. 54(31), 9157-9166,2015.

~~Pawan K Bhartia,~~ Pieternel F. Levelt, ~~Johanna Tamminen, et al. Recent results from the~~Gijsbertus H. J. van den Oord, Marcel R. Dobber, Anssi Mälkki, Huib Visser, Johan de Vries, Piet Stammes, Jens O. V. Lundell and Heikki Sarri. The Ozone Monitoring Instrument~~(OMI) on EOS Aura. SPIE, 6408: 64080Y-1-11~~. IEEE TRANSACTIONS AN GEOSCIENCE AND REMOTE SENSING. 44(5), 1093-1101, 2006.

P. S. Barry, J. Shepanski, C. Segal. Hyperion On-Orbit Validation of Spectral Calibration using Atmospheric Lines and an On-board System. Proc. Of SPIE, 4480:231-235, 2002.

Quintus Kleipool, Antje Ludewig, Ljubisa Babic, Rolf Bartstra, Remco Braak, Werner Dierssen, Pieter-Jan Dewitte, Pepijn Kenter, Robin Landzaat, Jonatan Leloux, Erwin Loots, Peter Meijering, Emiel van der Plas, Nico Rozemeijer, Dinand Schepers, Daniel Schiavini, Joost Smeets, Giuseppe Vacanti, Frank Vonk, and Pepijn Veefkind. Pre-launch calibration results of the TROPOMI payload on-board the Sentinel 5 Precursor satellite. Atmos. Meas. Tech. Discuss. Discussion started: 13 February 2018.

Robert A. Neville, Lixin Sun, Karl Staenz. Detection of spectral line curvature in imaging spectrometer data. SPIE, 5093:144-154, 2003.

Robert Voors, Johan de Vries, Ianjit S. Bhatti, Dan Lobb. TROPOMI, the Sentinel 5 precursor instrument for air quality and climate observations: status of the current design. International Conference on Space Optics-ICSO 2012.

Rosemary Munro, Rudiger Lang, Dieter Klaes, Gabriele Poli, Christian Retscher, Rasmus Lindstrot, Roger Huckle, Antoine Lacan, Michael Grzegorske, Andriy Holdak, Alexander Kokhanovsky, Jakob Livschitz, and Michael Eisinger. The GOME-2 instrument on the Metop series of satellites: instrument design, calibration, and level 1 data processing-an overview. Atoms. Meas. Tech., 9, 1279-1301, 2016.

Ruud Dirksen, Marcel Dobber, Pieternel Levelt, Gijsbertus van den Oord, Glen Jaross, Matt Kowalewski, George H. Mount, Don Heath, Ernest Hilsenrath and Johan de Vries, The on-ground calibration of the Ozone Monitoring Instrument from a scientific point of view, SPIE, 5234, 400-410, 2004.

Samuel F. Pellicori, Carol L. Martinez, Paul Hausgen, and David Wilt, Development and testing of coatings for orbital space radiation environments, Appl. Opt. 53, A339-A350, 2014.

S. Noel, H. Bovensmann, J. P. Burrows, et al. The SCIAMACHY instrument on ENVISAT-1. SPIE, 3498: 94-104, 1998.

S.Noel, A.A.Kokhanovsky, O.Jourdan, et al. SCIAMACHY REFLECTANCE AND SOLAR– IRRADIANCE VALIDATION. Proceedings of the Third Workshop on the Atmospheric Chemistry Validation of Envisat. 2006.

Xiaoxiong Xiong, Junqiang Sun, Xiaobo Xie,et al. On-orbit Calibration and Performance of Aqua MODIS Reflective Solar Bands. IEEE TRANSACTIONS ON GEOSCIENCE AND REMOTE SENSING, 48(1):535-546, 2009.

Xuemin Jin and Robert Y. Levine, Bidirectional reflectance distribution function effects in ladar-based reflection tomography, Appl. Opt. 48, 4191-4200, 2009.